University of Stavanger

Faculty of Science and Technology

MASTER'S THESIS

Study program/Specialization: Petroleum Engineering/Drilling	Spring semester, 2014 Open
Writer: Maria Sletteng Johnsen	..... (Writer's signature)
Faculty supervisors: Rune W. Time Hermonja A. Rabenjafimanantsoa	
Title of thesis: Particle Transport and Hole Cleaning in Wells During Drilling	
Credits (ECTS): 30	
Key words: Particle transport Hole cleaning PIV Falling spheres Terminal velocity	Pages: 63 + enclosure: 24 + DVD Stavanger, 16.06.14

Particle Transport and Hole Cleaning in Wells During Drilling

Master's thesis spring 2014

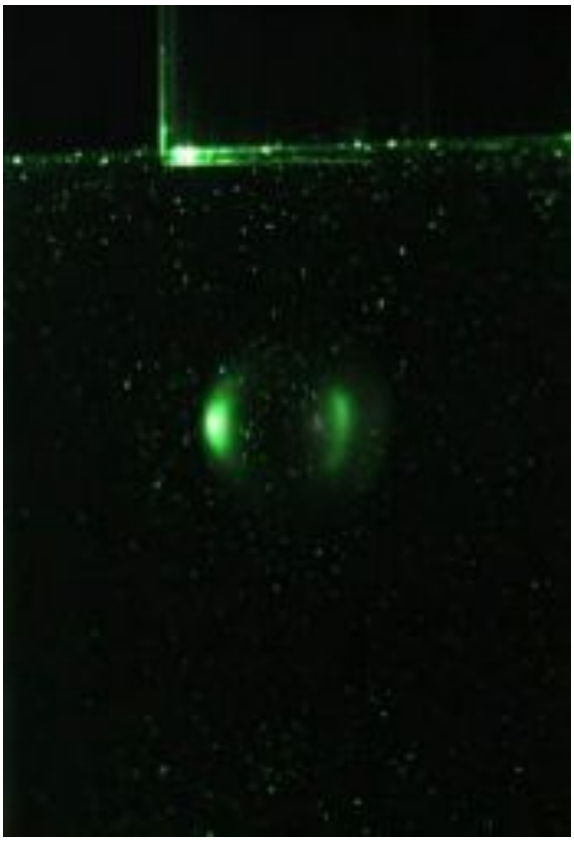

Maria Sletteng Johnsen

Department of Petroleum Engineering

Faculty of Science and Technology

University of Stavanger

16.06.14

Summary

The purpose of the thesis was to look at particles in different rheology to develop a methodology for measuring settling velocities in static systems. There was built a small-scale cell with an inner pipe and a discharge system. In advance there was done a feasibility test on which particles to use. As a result of this test, it was decided to use glass beads with the diameter of 0.001 m, 0.002 m and 0.003 m, and steel spheres with the diameter of 0.004 m and 0.015 m.

The fluids used were water and PAC in order to compare behavior in Newtonian versus non-Newtonian fluids. Two different concentrations of PAC were used. Rheology and density measurements were done prior to the experiment. PAC-4g/l was heavier and more viscous than water, and PAC-8g/l was heavier and more viscous than PAC-4g/l.

The terminal velocity of the particles was determined by theoretical formulas found from literature and by looking at pictures from the camera recordings. Both regular and high-speed camera was used. The results from the experiment in water are presented below and show that the experimental velocity is coherent with the theoretical velocity.

Table 1: Terminal velocities in water

d $[m]$	$v_{t,t}$ $[m/s]$	$v_{t,e}$ $[m/s]$
0.001	0.2254	0.1903
0.002	0.2879	0.2828
0.003	0.3691	0.3955
0.004	0.9453	0.9872
0.015	1.665	1.610

There was done a second feasibility test on the fluids with different rheology. The velocities and movements of particles of each size were studied, both in single and cluster movements. Here it was ascertained that the velocity decreases with increasing viscosity of the fluid. It was also observed that particles moving together in clusters have a higher velocity than a single particle. As a result of this test, it was decided to look at a two-phase system, where Bayol 35 was used as an oil solution and PAC-4g/l was used as a water solution. The results from this experiment showed similar velocities as previously found for water and PAC.

Contents

Preface

The master's thesis was written as a part of the completion of a 5-year long petroleum engineering study and is weighted with 30 credits. I chose to write my thesis for the University of Stavanger because I was offered an experimental task that I thought was very interesting. Also, the Department of Petroleum Engineering has dedicated supervisors who have been able to pass on valuable knowledge and have provided excellent guidance.

As a part of my work I would like to thank the following people:

Senior Engineer Hermonja A. Rabenjafimanantsoa, Benja, who created a good atmosphere, motivated me and was of excellent guidance during the construction and the final part of my work.

Professor Rune W. Time, for his excellent guidance, knowledge, good comments and for providing Matlab programs and equipment in relation to the high-speed recordings.

Head Engineer Kim Andre Nesse Vorland, for guidance in the use of the rheometer.

Family and friends, my sincere gratitude goes out to you for encouragement and support throughout these 5 years, which has given me the motivation to realize this achievement.

Nomenclature

Abbreviations

CMC	Carboxymethyl Cellulose
DEM	Discrete/Distinct Element Method
FPS	Frames per second
PAC	Polyaniotic Cellulose
PAC-4g/l	4 g PAC/l dissolved in water
PAC-8g/l	8 g PAC/l dissolved in water
PIV	Particle Image Velocimetry

Roman letters

C_d	Drag coefficient
d	Particle diameter
d_b	Base diameter
d_T	Throat diameter
f	Drag factor
g	Acceleration
h_c	Height of cell
h_p	Height of inner pipe
I_1	Interrogation area from frame 1
I_2	Interrogation area from frame 2
K	Consistency index
l	Length of cell
n	Power law index
m	Consistensy index, Chhabra
Re	Reynolds number
$S\tau_V$	Stokes number related to the particle velocity
t	Time
u	Velocity in x-direction
v	Velocity in y-direction
v_t	Terminal velocity
$\bar{x}$	Particle displacement

Greek letters

α_d	Volume fraction
γ	Shear rate
μ	Viscosity
μ_c	Viscosity of the continuous phase
μ_l	Fluid viscosity
ρ_p	Particle density
ρ_l	Fluid density
σ	Deviation
τ	Shear stress
τ_C	Average time between particle-particle collition
τ_F	Time characteristic of the flow field
τ_V	Momentum (velocity) response time

Subscripts

e	Experimental
PL	Power law
PS	Pseudoplastic
r	Relative
t	Theoretical

List of Figures

List of Tables

Chapter 1

Introduction

Drilling can be described simply as "the removal of rock from its current position and subsequent transportation by drilling fluid to the surface for disposal". The removal of cuttings from the well is one of the most important functions of drilling fluids. Efficient removal can insure longer bit life and greater efficiency in drilling. When the cuttings are circulated towards the surface, the cuttings tend to sink through the ascending fluid due to the influence of gravity. The velocity of this sinking process is known as the settling velocity or terminal velocity.

The settling velocity of any particle is dependent on many factors such as density and viscosity of the fluid, the volume, specific gravity, shape and roughness of the particle. In this thesis, the objective is to develop a methodology for measuring settling velocities in fluids with different rheology. It is desirable to study particles of different material and various sizes.

An existing small-scale cell has been built, but has not been used before. A part of this project is to modify the cell and to develop a technique to set up representative conditions for the measurements.

There has been developed a Matlab program, which can calculate the theoretical velocity of the particles. With the results from this program, one has the opportunity to compare this to the obtained experimental terminal velocity and discuss how coherent they are.

After the modifications were done, the cell was filled with water and the motion of the particles was recorded by a camera. The data was then analyzed in various programs and the experimental velocity was obtained. PIV analyses were also performed.

The experiments with the fluids of different rheology were done in a graduated cylinder. There were used two concentrations of a polymer solution. An two-phase system with oil and water was also studied in the same graduated cylinder.

As preparation to this thesis, there were read different articles and books concerning terminal velocity and drag forces on particles under various conditions to gain background knowledge and a better understanding. An important part of the experiment was to study the settling velocities with different particles at different rheologies. A lot of useful information and inspiration was taken from the book Multiphase Flows with Droplets and Particles" written by C. Crowe, J. Schwarzkopf, M. Sommerfeld and Y. Tsuji.

The thesis is organized as follows:

Chapter 2 describes the theory related to this experiment. It concerns topics like hole cleaning, properties of dispersed phase flows, particle interactions and particle image velocimetry.

Chapter 3 includes two feasibility tests. The first test deals with particles studied in a microscope and the second test deals with velocity in fluids of different rheology.

Chapter 4 describes the experimental setup regarding the construction, use of PIV, two-phase system, fluid rheology, description of equipment and programs used.

Chapter 5 presents the results from the experiments, including rheology and density measurements, terminal velocities and PIV analyses.

Chapter 6 concludes the experiments.

Appendices A, B and C covers various results, Matlab scripts and illustrations, respectively.

Chapter 2

Theory

2.1 Hole cleaning

Hole cleaning is the ability of a drilling fluid to suspend drilled cuttings and transport them from downhole to the surface. It is among the most important problems to handle in drilling operations and poor hole cleaning can lead to costly drilling problems, such as:

- Mechanical pipe sticking
- Premature bit wear
- Slow drilling
- Formation fracturing
- Excessive torque and drag on drill string
- Difficulties in logging and cementing
- Difficulties in casing landing

Several factors can affect hole cleaning efficiency. Annular-fluid velocity; the flow rate is the main factor in cuttings removal while drilling directional wells. An increase in flow rate will result in more efficient cuttings removal under all conditions [1].

Inclination angle is a challenge in directional wells and extended reach drilling operations. Experience has shown that deviated wells with hole angles of 40-65° are the most difficult to clean. This is due to the tendency of cuttings to form beds and to slide back down into the hole. The cuttings bed causes the flow-rate requirement to increase [6].

The characteristics of the cuttings also have a significant effect of enhancing hole cleaning. The size, distribution, shape, and specific gravity of cuttings affect their dynamic behavior in a flowing media. The specific gravity of most rocks is approximately 2.6, therefore, specific gravity can be considered a non-varying factor in

cuttings transport. The cuttings size and shape are functions of the bit types being used. Smaller cuttings are more difficult to transport in directional-well drilling, however, with some viscosity increase and pipe rotation, fine particles seem to stay in suspension and are easier to transport [6].

Other hole cleaning factors are drill string rotation, hole eccentricity, rate of penetration and mud properties. Figure 2.1 demonstrates the process of a hole cleaning in a vertical well [1].

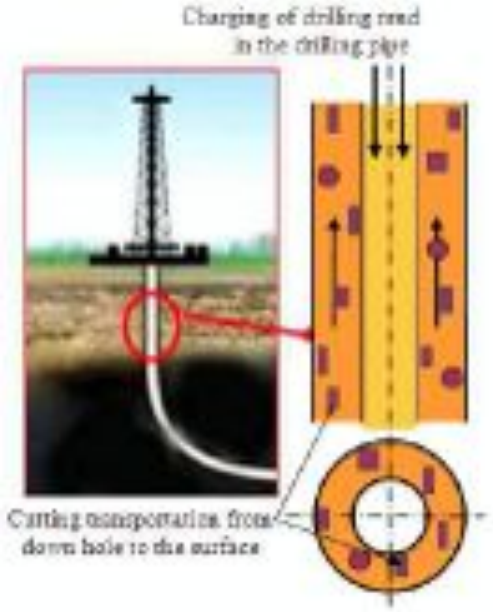

Figure 2.1: Drilling mud charging and cuttings upward transportation [1]

2.2 Fluids

2.2.1 Newtonian fluids

A newtonian fluid is a fluid which exhibits a linear relation between the applied shear stress, τ and the shear rate γ. The relation is given by

$$\tau = \frac{F}{A} = \mu\gamma \tag{2.1}$$

where the proportionally constant μ is the viscosity of the fluid. A representation of this relation can be found as the black curve in Figure 2.2. In Newtonian fluids, the viscosity is only temperature and pressure dependant [7]. An example of a Newtonian fluid is water, which was used in this thesis.

2.2.2 Non-Newtonian fluids

A non-Newtonian fluid is a fluid which exhibits a non-linear relation between the applied shear stress, τ, and shear rate, γ. In non-Newtonian fluids, the viscosity, in

addition to temperature and pressure, is shear stress and shear rate dependant [7].

There are mainly three types of non-Newtonian fluids. Figure 2.2 shows the comparison between these fluids relative to a Newtonian fluid.

- Plastic. Shear-thinning fluids, which means that the viscosity decreases as the shear rate increases.
- Pseudoplastic. Also shear-thinning fluids, but the transition between plastic and pseudoplastic can be hard to distinguish.
- Dilatant. Shear-thickening fluids, which means the viscosity increases as the shear rate increases.

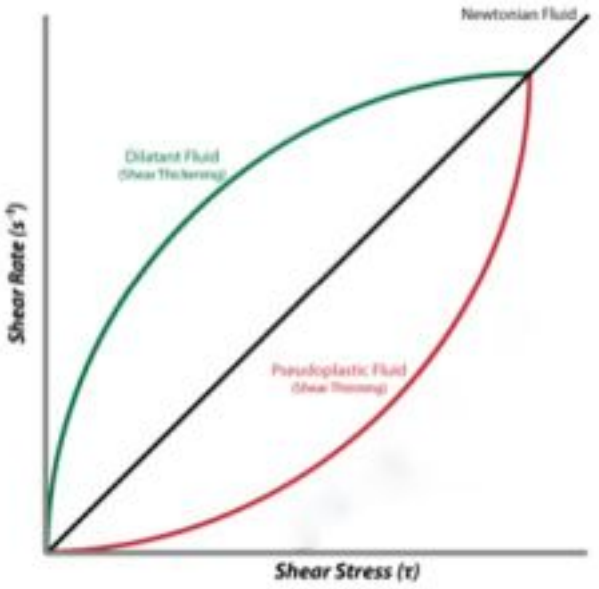

Figure 2.2: Comparison of Newtonian and non-Newtonian fluids [2]

Power law is one of the models that have been developed to describe fluids. Power law gives a good description of the relation between shear stress and shear rate for pseudoplastic fluids. The advantage of using the Power law is that any shear rate can be used, and especially at low shear rates it gives a good description of the fluid flow properties. The model is described by [7]

$$\tau = K \cdot (\dot{\gamma})^n \tag{2.2}$$

or

$$log(\tau) = logK + n \cdot log(\dot{\gamma}) \tag{2.3}$$

n and K are dervied from equation 2.3

$$n = \frac{log\frac{(\tau_1)}{(\tau_2)}}{log\frac{(\dot{\gamma}_1)}{(\dot{\gamma}_2)}} \tag{2.4}$$

$$K = \frac{\tau}{\dot{\gamma}^n} \tag{2.5}$$

The Power law describes three flow models, categorized by the n-value:

- Newtonian when n = 1
- Pseudoplastic when n < 1
- Dilatant when > 1

Polyaniotic Cellulose (PAC) is an example of a non-Newtonian fluid and was used in this thesis. PAC is a cellulose derivative polymer, and when added to water, it becomes a shear-thinning fluid. PAC can be used to increase the viscosity of a fluid, and this ability was used to make different concentrations of the fluid. PAC is transparent, which is the main reason why it was used in this thesis. Since all of the observations of the experiments are based on camera-recordings, a transparent fluid is a necessity.

2.3 Properties of dispersed phase flows

2.3.1 Response time

The time it takes for a particle to respond to changes in flow velocity is called the momentum response time. This response time is important when it comes to establishing non-dimensional parameters to characterize the flow. For the limits of low Reynolds numbers, which implies Stokes flow, the drag factor approaches unity and the momentum response time can be defined as

$$\tau_V = \frac{\rho_d d^2}{18\mu_c} \tag{2.6}$$

Where ρ_d is the density of the particle, d is the diameter of the particle and μ_c is the viscosity of the continuous phase [3].

2.3.2 Stokes number

The Stokes number is a very important parameter in fluid-particle flows. The Stokes number related to the particle velocity is defined as

$$S\tau_V = \frac{\tau_V}{\tau_F} \tag{2.7}$$

Where τ_F is time characteristic of the flow field. For example, the characteristic time for the flow through a venturi may be d_T/u where d_T is the throat diameter and u is the flow velocity. The Stokes number then becomes

$$S\tau_V = \frac{\tau_V u}{d_T} \tag{2.8}$$

If $S\tau_V \ll 1$, the response time of the particles is much less than the characteristic time associated with the flow field. The particles will then have enough time to respond to the changes in flow velocity. If $S\tau_V \gg 1$, the particle will have no time to respond to the fluid velocity changes and the particle velocity will be little affected during it passage through the venturi [3].

2.3.3 Dilute vs. dense flows

A dilute dispersed phase flow is a flow where the particle motion is controlled by the fluid forces such as drag and lift. A dense flow is a flow where the particle motion is controlled by collisions or continuous contact between the particles. An approximate estimate of whether the flow is dilute or dense can be made by studying the ratio of momentum response time of a particle to the time between collisions. The flow is considered dilute if

$$\frac{\tau_V}{\tau_C} < 1 \tag{2.9}$$

where τ_C is the average time between particle-particle collisions because the particles have sufficient time to respond to the local fluid dynamic forces before the next collision. The flow is considered dense if

$$\frac{\tau_V}{\tau_C} > 1 \tag{2.10}$$

since then the particle has no time to respond to the fluid dynamic forces before the next collision.

There are many mechanisms that are responsible for particle-particle collisions so it is difficult to establish the limits of dilute and dense flows. However, the magnitude of the particle volume fraction, α_d, can give a general indicator as shown in Figure 2.3.

For particle volume fractions < 0.001, the flow can be considered as dilute. The dense flow is separated into collision-dominated and contact-dominated regimes. A collision-dominated flow is when the particles collide and the path of the particles is changed. The time during collision is small compared to the time between collisions. The particle volume fraction of a collision-dominated flow lie between 0.001 and 0.1. A contact-dominated flow is when the particles are in continuous contact and contact forces are responsible for the particle motion. The particle volume fraction for contact-dominated flow is 0.1 or greater [3].

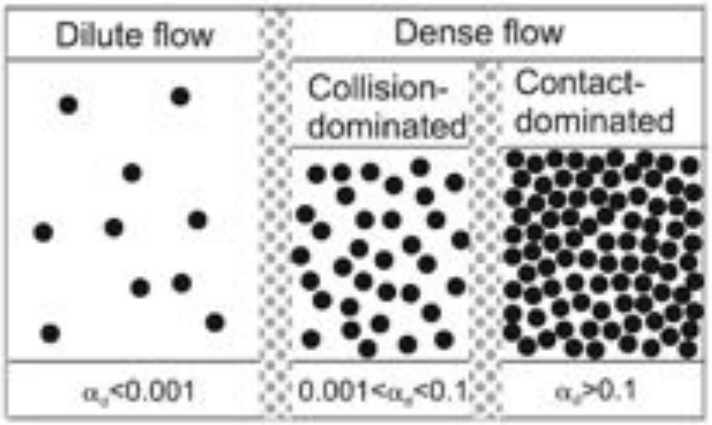

Figure 2.3: Flow regimes for dilute and dense flows [3]

2.4 Particle interactions

2.4.1 Drag forces

The drag coefficient is an important hydrodynamic characteristic of the motion of particles in both Newtonian and non-Newtonian fluids. In general, the drag coefficient, will depend on the particle shape and orientation with respect to the flow as well as on the flow parameters such as Reynolds number, Mach number, turbulence level etc. The most fundamental configuration is the sphere. The variation of the drag coefficient with the Reynolds number for a non-rotating sphere is shown in Figure 2.4. This variation is known as the standard drag curve [3].

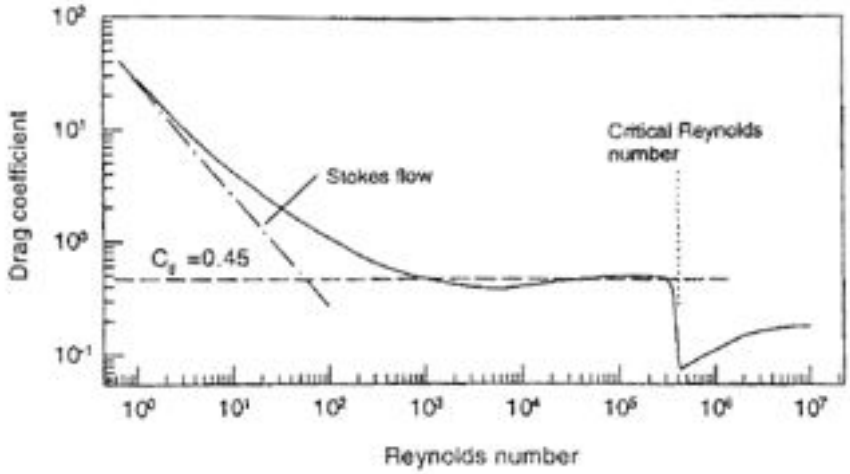

Figure 2.4: Variation of the drag coefficient of a sphere with Reynolds number [3]

At low Reynolds numbers the drag coefficient varies inversely with the Reynolds number. This is referred to as the Stokes flow regime. With increasing Reynolds number the drag coefficient approaches a nearly constant value, which is known as the inertial range. For $750 < \mathrm{Re} < 3.5{\times}10^5$ the drag coefficient varies only 13 % from $C_d = 0.445$. With increasing Reynolds number there is a sudden decrease in

drag coefficient at the critical Reynolds number [3].

The drag coefficient can be defined as

$$C_d = \frac{24}{Re_r} \tag{2.11}$$

where Re_r is the Reynolds number based on the relative velocity

$$Re_r = \frac{\rho_l v d}{\mu_l} \tag{2.12}$$

Equation 2.12 is the classic stokes drag coefficient which is valid for $Re_r < 1$ [3].

Matijašić and Glasnović [8] have done a study on drag coefficient in pseudoplastic fluids, which is similar to the non-Newtonian part of this thesis. They used CMC aqueous solutions with different rheology, and particles of different sizes and material.

Considering spherical particles falling in fluids, Newtons law can be used for evaluation of drag coefficient in laminar, transition and turbulent region.

$$Cd = \frac{4(\rho_p - \rho_l)gd}{3\rho_l {v_t}^2} \tag{2.13}$$

Those values were corrected for the value of wall effect. Particle Reynolds number was calculated using equation 2.13 modified for Power-law (pseudoplastic) fluids.

$$Re_{PS} = \frac{v_t 2 - n d^n \rho_l}{K} \tag{2.14}$$

Drag coefficients for laminar and transition flow were found, but there was need for a model that correlates better with experimental results at higher values of Reynolds number. Mathematical regression of experimental data resulted with simplification of the drag coefficient correction factor as

$$Cd = \frac{24}{Re_{PS}} \cdot A(n) + 0.653 \tag{2.15}$$

where

$$A(n) = -1.26n + 2.3 \tag{2.16}$$

The obtained empirical correlation is applicable in a wider range of Reynolds number, $Re_{PS} < 1000$ [8].

Chhabra [9] has also done several studies on drag coefficient and Power-law fluids. He describes the Reynolds number as

$$Re_{PL} = \frac{\rho v^{2-n} d^n}{m} \tag{2.17}$$

where m is the consistency index (K).

The drag coefficient, Cd, can then be desribed as

$$Cd = \frac{24}{Re_{PL}} \cdot 3^{2n-3} \cdot \frac{n^2 - n + 3}{n^{3n}} + \frac{4n^4}{24Re_{PL}^{\frac{n-3}{3}}} \tag{2.18}$$

2.4.2 Terminal velocity

The terminal velocity, v_t, is the final velocity a particle attains falling in a quescent fluid (u = 0). The equation of motion for a particle or droplet using the steady-state drag coefficient can be expressed as

$$m\frac{dv}{dt} = 3\pi\mu_c df(u - v) + mg \tag{2.19}$$

where g is the acceleration due to gravity, v is positive in the direction of gravity (downward), and f is the drag factor or the ratio of the drag coefficient to Stokes drag

$$f = \frac{C_d Re_r}{24} \tag{2.20}$$

Assuming a spherical droplet with material density of ρ_p, equation 2.13 can be written as

$$m\frac{dv}{dt} = \frac{f}{\tau_V}(u - v) + g \tag{2.21}$$

where τ_V is the velocity response time.

There are several correlations for f as a function of Reynolds number. One correlation is described by Clift and Gauvin and can be expressed by

$$f = 1 + 0.15Re_r^{0.687} + 0.0175(1 + 4.25 \times 10^4 Re_r^{-1.16})^{-1} \tag{2.22}$$

This correlation provides a fit for f within $\pm 6\%$ of the experimental value over the entire subcritical Reynolds number range.

Once the particle has achieved terminal velocity there is no more acceleration, so the terminal velocity is described as [3]

$$v_T = \frac{g\tau_V}{f}(1 - \frac{\rho_c}{\rho_d}) \tag{2.23}$$

2.4.3 Particle-particle interaction

Particle-particle interaction controls the motion of the particles in dense particle flows. As the particle concentration becomes higher, particles collide with each other and the loss of particle kinetic energy due to inter-particle collision cannot be neglected. With respect to particle-particle interactions in multiphase flow dynamics, two phenomena are identified: collision and contact. From the viewpoint of physics, collision and contact do not differ significantly. Collision is merely contact with short time duration, however the modeling approach is different for each. For collision or

contact, two models are normally used, the hard sphere model and the soft sphere model [3]. The collision of two particles is shown in Figure 2.5.

The hard sphere model is based on the impulsive force, which is defined by the integral of the force acting on a particle versus time. With the hard sphere model the post-collisional velocities and rotations are determined as a function of the pre-collisional conditions, coefficient of restitution and coefficient of friction [3].

The soft sphere model describes the particle history during the collision process and is modeled by using mechanical elements such as spring and a dash-pot. The soft sphere model is also called DEM (Discrete Element Method or Distinct Element Method) [3].

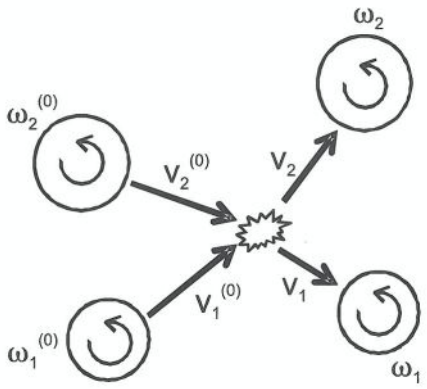

Figure 2.5: Particle-particle collision [3]

2.4.4 Particle-wall interaction

The problem of particle-wall interaction is encountered when analyzing fluid-particle flows contained within walls such as pipe flows, channel flows and fluidized beds. The particle-wall interaction falls into two categories: hydrodynamic interaction due to the proximity of a wall and mechanical interaction caused by contact with the wall [3].

An example of the hydrodynamic interaction is the Saffman lift force due to velocity gradient near the wall. Another example is the fluid force acting on the particle approaching the wall in the normal direction [3].

The treatment of the mechanical behavior associated with particle-wall interaction depends on the inertia of the particle. When a massive particle collides with a wall, it rebounds but loses kinetic energy due to friction and inelasticity effects. For a very small particle approaching a wall, molecular forces become dominant compared to the inertial forces. As a result, the particle is captured by the wall due to cohesive forces, and neither rebounds from nor slides along the wall. This cohesive force is identified as the van der Waals force [3]. The collision of particles and a wall is shown in Figure 2.6.

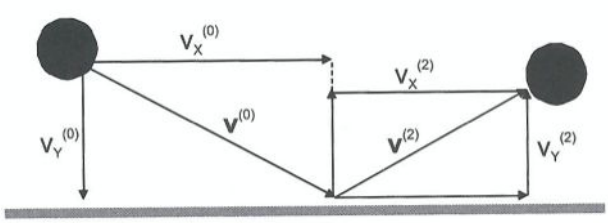

Figure 2.6: Particle-wall collision [3]

The symbol **v** signifies the translation velocity. The velocity has two components: longitudinal component (x-component) and the component normal to the wall (y-component) [3].

2.5 Particle image velocimetry (PIV)

PIV is a non-intrusive laser optical measurement technique for research and diagnostics into flow, turbulence, microfluidics, spray atomization and combustion processes. There are several PIV measuring methods. Standard PIV measures two velocity components in a plane using a single camera whereas Stereo PIV uses two cameras to measures three velocity components in a plane. Time resolved PIV is the measuring method being used in the experiment, which is executed with a high-speed camera at a fixed frame rate [10].

The principle behind PIV is that the velocity vectors are derived from sub sections of the target area of the particle-seeded flow by measuring the movements of particles between two light pulses:

$$V = \frac{\triangle \bar{x}}{\triangle t} \tag{2.24}$$

The flow is illuminated in the target area with a light sheet. The camera lens images the target area onto the sensor array of a digital camera. The camera is able to capture each light pulse in separate image frames. Once a sequence of two light pulses is recorded, the images are divided into small subsections called interrogation areas. The interrogation areas from each image frame, I_1 and I_2, are cross-correlated with each other, pixel by pixel. The correlation produces a signal peak, identifying the common particle displacement, $\triangle \bar{x}$. An accurate measure of the displacement - and thus also the velocity - is achieved with sub-pixel interpolation. A velocity vector map over the whole target area is obtained by repeating the cross-correlation for each interrogation area over the two image frames captured by the camera [4].

Figure 2.7 shows the measurement principle of PIV illustrated by Dantec Dynamics. Please note that a continous laser was used in the experiment, not a double-pulsed laser as shown in the figure.

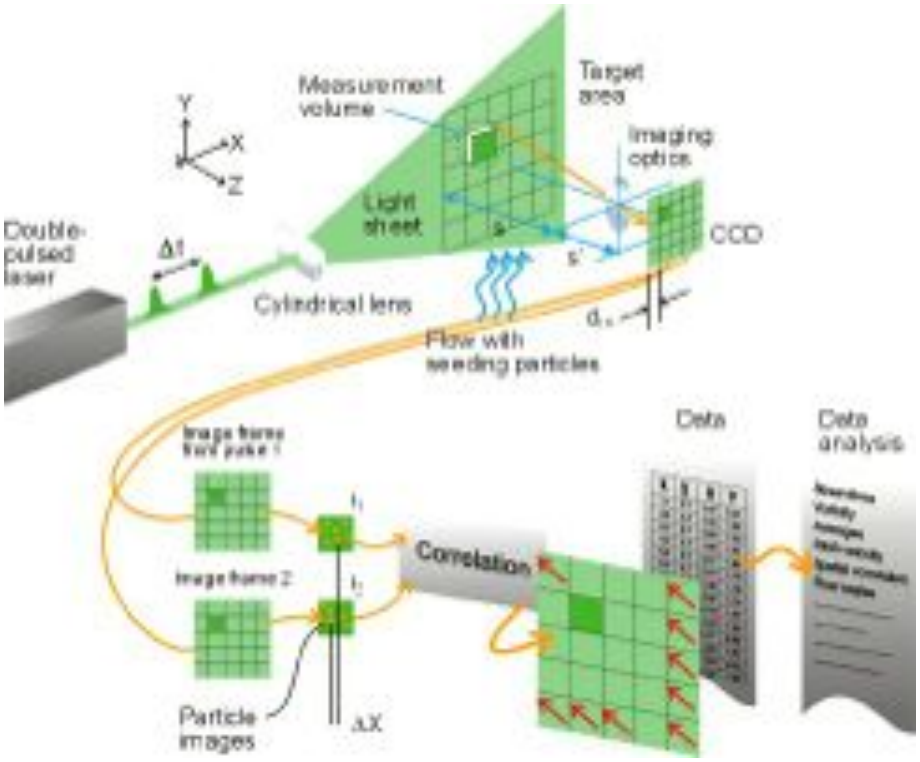

Figure 2.7: Measurement principle of PIV [4]

Chapter 3

Feasibility tests

3.1 Procedures

There were done two feasibility tests; one on particles in a microscope and one on particles in fluids with different rheology.

The first feasibility test was done in advance of the experiments and regarded the different particles. The purpose of this test was to verify the given diameters of the particles, if they were spherical and if they contained any visible air. This was important due to the problem of unwanted buoyancy that might have been caused by void spaces in the particles.

Particles available were glass beads with the diameter of 0.0002 m, 0.0005 m, 0.001 m, 0.002 m, 0.003 m and steel spheres with the diameter of 0.004 m and 0.015 m. The material of the particles is hereinafter abbreviated in tables to g and s, describing glass and steel, respectively.

First, there was done a study with an USB 2.0 MP microscope with camera from Normet/Teknika, but the quality of the pictures were poor and it was hard to determine if the particle contained air or not. Afterwards, there was done a study with a Carl Zeiss Stemi 2000-C microscope with a Carl Zeiss AxioCam ERc 5s camera. This microscope was much better and the quality of the pictures was good. The diameter of the particles was verified by placing them on an EMO A4 graph paper. The weight of the particles was determined using a Sartorius Extend ED224S analytical weight. The volume and density of the particles was then calculated. Illustration of the different equipment used in this feasibility tests is shown in Figure 3.1.

(a) Carl Zeiss Stemi 2000-C microscope

(b) Sartorius Extend ED224S analytical weight

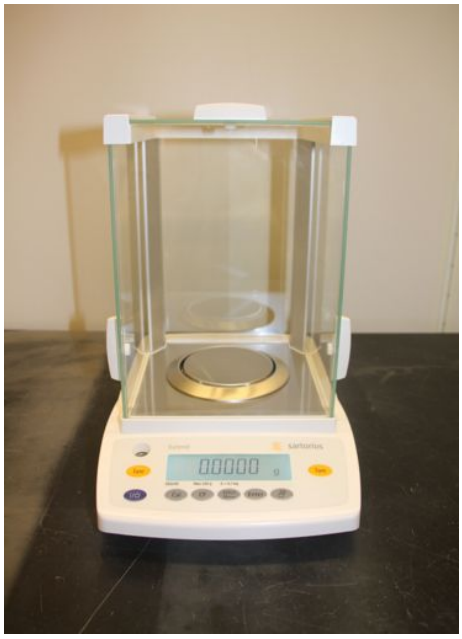

Figure 3.1: Feasibility test equipment

The next feasibility test was done after the experiments with water and regarded the fluids with different rheology. The purpose of this test was to see if the selected concentrations of PAC were suitable to use in the experiment. It was desirable to see the behavior of the particles when many were dropped together, whether the flow was dilute or dense. It was also desirable to obtain an estimation of the velocities of the various particles in PAC.

1 liter of PAC-4g/l and 1 liter PAC-8g/l was made. Description of the method and equipment can be found in chapter 4.2. The fluid was placed in a graduated cylinder with a volume of 1 liter. The particles were first lowered to the surface of the fluid using a spoon, to become saturated. To avoid any additional forces exerted on the particles, they were dropped from this height afterwards. This sequence was done with the glass bead particles of 0.001 m, 0.002 m and 0.003 m in both water, PAC-4g/l and PAC-8g/l and was recorded by the Samsung camera. The experimental results for PAC-4g/l were then compared to the theoretical results from the Matlab program "Kulefall non-Newtonian".

3.2 Results

In the first feasibility test it was determined to examine ten particles of each diameter to obtain statistics. This does not apply to the 0.015 m steel sphere, as there was only one single sphere of that size available. Also, this steel sphere was too big to be analyzed in a microscope so the diameter was determined using a caliper. A short overview of the results is shown in Table 3.1, and the full statistics can be found in Appendix A.

Table 3.1: Properties of the different particles

#	Material	Diameter $[m]$	Weight $[kg]$	Volume $[m^3]$	Density $[kg/m^3]$
1	g	1.000E-03	2.150E-06	5.233E-10	4.108E+03
2	g	2.000E-03	1.149E-05	4.187E-09	2.744E+03
3	g	3.000E-03	3.666E-05	1.413E-08	2.594E+03
4	s	4.000E-03	2.535E-04	3.349E-08	7.568E+03
5	s	1.500E-02	1.367E-02	1.766E-06	7.740E+03

From the photos of the second feasibility test it was observed that the flow of particles in water was dilute, this applied to all of the different diameters. A photo of the dilute flow for the 0.003 m glass beads can be seen in Figure 3.2. Regarding the velocity of the particles, the results were similar to the prior experiments done in water in the cell. The particle with the smallest diameter had the slowest velocity. It was also seen that the particles falling in clusters had a slight higher velocity than a single particle alone. The properties of the different particles falling in water are presented in Table 3.2.

Table 3.2: Properties of particles falling in water

#	Material	Diameter $[m]$	Velocity $[m/s]$	Flow
Cluster	g	1.000E-03	1.708E-01	Dilute
1	g	1.000E-03	1.250E-01	-
Cluster	g	2.000E-03	2.589E-01	Dilute
1	g	2.000E-03	2.539E-01	-
Cluster	g	3.000E-03	3.381E-01	Dilute
1	g	3.000E-03	3.194E-01	-

In PAC-4g/l it was seen that the flow of particles was dense, and this also applied to all of the different diameters. It is assumed that the dense flow is a result of the attraction between the particles caused by gel and the viscous effects. A photo of the dense flow for the 0.003 m glass beads is shown in Figure 3.3. Similar to the particles falling in water, the particle with the smallest diameter had the slowest velocity and the particles falling in clusters had a higher velocity than a single particle alone. Due to the high viscosity of PAC-4g/l, the overall velocities of the particles were much slower than for the ones in water. The properties of the different particles falling in

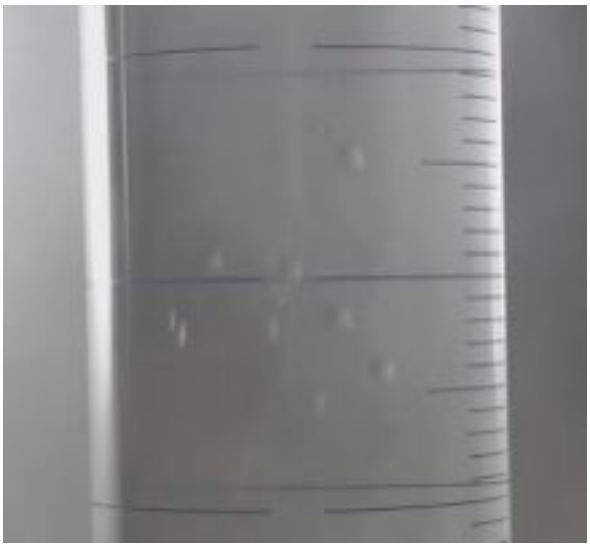

Figure 3.2: Dilute flow of 0.003 m glass beads in water

PAC-4g/l are presented in Table 3.3.

Table 3.3: Properties of particles falling in PAC-4g/l

#	Material	Diameter $[m]$	Velocity $[m/s]$	Flow
Cluster	g	1.000E-03	5.969E-02	Dense
1	g	1.000E-03	3.353E-03	-
Cluster	g	2.000E-03	8.737E-02	Dense
1	g	2.000E-03	3.352E-02	-
Cluster	g	3.000E-03	1.695E-01	Dense
1	g	3.000E-03	5.362E-02	-

In PAC-8g/l the results were very similar to the ones for PAC-4g/l, except that the velocities were even slower than for PAC-4g/l, due to a higher viscosity. The flow was also dense and the particles falling in clusters had a higher velocity than the single particles. A photo of the dense flow for the 0.003 m glass beads is shown in Figure 3.4. The properties of the different particles falling in PAC-8g/l are presented in Table 3.4.
The experimental results for PAC-4g/l were compared to the theoretical results. Two models were used, Chhabra and Matijašić, and two different rheologiy measurements were used. It was decided to use two models to see if they gave different results. It was also interessting to see if or how much the variation in the Power law values would affect the results, so it was decided to enter values for two rheology measurements. Power law values for shear rate 1020 s^{-1} and 1 s^{-1} were studied. Table 3.5 shows the comparison of experimental and theoretical velocities, based on values for the 1020 s^{-1} shear rate. The Power law values for this measurement is n = 0.6 and K= 0.5.

Figure 3.3: Dense flow of 0.003 m glass beads in PAC-4g/l

Table 3.4: Properties of particles falling in PAC-8g/l

#	Material	Diameter $[m]$	Velocity $[m/s]$	Flow
Cluster	g	1.000E-03	1.332E-02	Dense
1	g	1.000E-03	1.710E-03	-
Cluster	g	2.000E-03	1.518E-02	Dense
1	g	2.000E-03	2.692E-02	-
Cluster	g	3.000E-03	2.949E-01	Dense
1	g	3.000E-03	6.543E-02	-

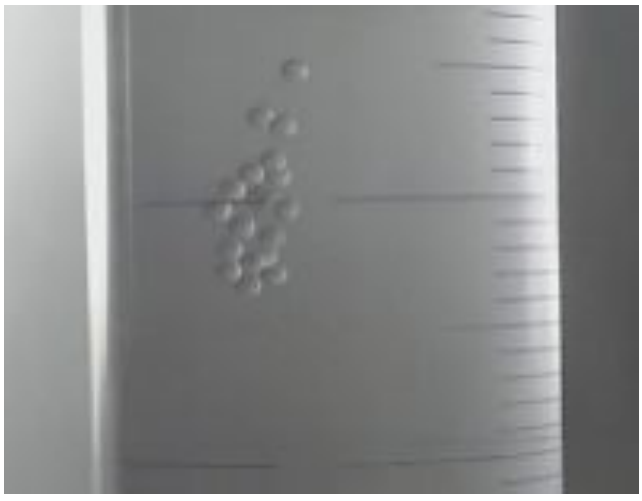

Figure 3.4: Dense flow of 0.003 m glass beads in PAC-8g/l

It is seen that the models give different results compared to the experimental value and they are not particularly coherent with each other either. For the 0.001 m

Table 3.5: Comparison of experimental and theoretical velocities for Power-law values from shear rate of 1020 s^{-1}

d $[m]$	$v_{t,e}$ $[m/s]$	$v_{t,Chhabra}$ $[m/s]$	$v_{t,Matijasic}$ $[m/s]$
1.000E-03	3.353E-03	8.184E-03	3.703E-03
2.000E-03	3.352E-02	1.969E-02	8.963E-03
3.000E-03	5.362E-02	4.880E-02	2.359E-02

particle the Matijašić model is closest to the experimental value, but for the 0.003 m particle the Chhabra model is the closest. In Figure 3.5 the velocity components for both models is shown for the 0.001 m particle. The velocity is displayed on the y-axis and is given in m/s. Time is shown on the x-axis and is given in seconds. From the figure one can see that the velocity in x-direction is zero for both models. The particle obtained its terminal velocity in the y-direction approximately after 0.04 s for Chhabra and after 0.02 s for Matijašić. The velocity is given as a negative value because the particle is going downward. The plots for the 0.002 m and 0.003 m particle have different values, but follow the same trend so these plots are omitted.

(a) Chhabra (b) Matijasic

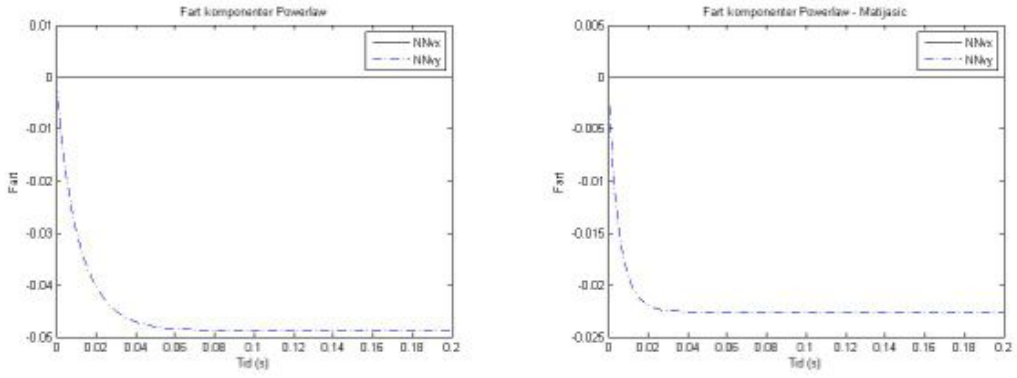

Figure 3.5: Velocity components for the 0.001 m glass bead, based on Power-law values from shear rate of 1020 s^{-1}

Table 3.6 shows the comparison of experimental and theoretical velocities, based on values for the 1 s^{-1} shear rate. The Power law values for this measurement is n = 0.9 and K= 0.2.

Table 3.6: Comparison of experimental and theoretical velocities for Power-law values from shear rate of 1 s^{-1}

d $[m]$	$v_{t,e}$ $[m/s]$	$v_{t,Chhabra}$ $[m/s]$	$v_{t,Matijasic}$ $[m/s]$
1.000E-03	3.353E-03	1.016E-02	9.041E-03
2.000E-03	3.352E-02	2.241E-02	2.045E-02
3.000E-03	5.362E-02	4.515E-02	4.291E-02

It is seen that the models give different results from these rhology values too, but in this case the models are more coherent with each other. For the 0.001 m particle, none of the models fit the experimental value very well. For the 0.002 m and 0.003 m particles the models are very coherent with each other and they show a closer theoretical value compared to the experimental value. The fit is still not very good, but the results from this shear rate are better than the ones for the 1020 s^{-1} shear rate.

In Figure 3.6 the relation of drag coefficient vs. Reynolds number for the 0.001 m particle is shown. The figure shows both models and the plots are based on rheology values for shear rate of 1 s^{-1}. The drag coefficient is shown on the y-axis and the Reynolds number is shown on the x-axis. For the Chhabra model, the curve riser quickly and has its peak where the drag coefficient is approximately 3400 and the Reynolds number is approximately 0.01. From then on the curve goes down and ends with a drag coefficient value of 500 and a Reynolds number of 0.065. The curve for the Matijašić model is very similar, but with different values. This curve has its peak where the drag coefficient is 3750 and the Reynolds number is slightly below 0.01. The curve ends with a drag coefficient value of 500 and a Reynolds number of 0.055.

(a) Chhabra

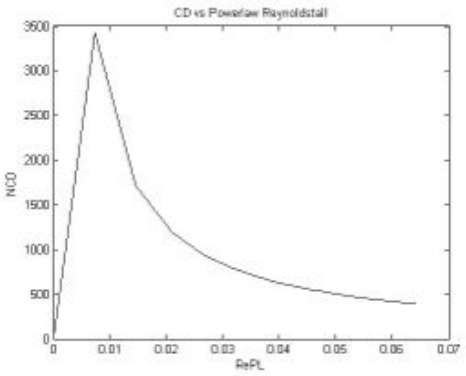

(b) Matijasic

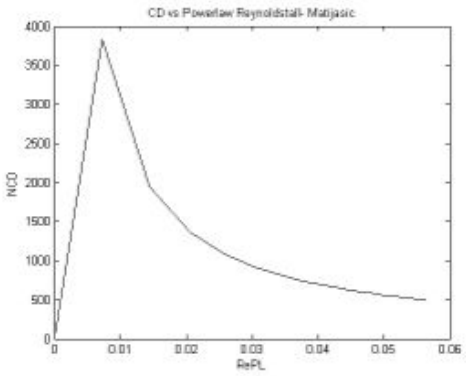

Figure 3.6: Drag coefficient vs. Reynolds number for Power-law values from shear rate of 1 s^{-1}

When comparing the models based on the different rheology values, one can see that there is a big difference in values for the each shear rate. The Chhabra model gives the least variation in results between the shear rates, and is the model that fits

the experimental values best. The Matijašić model shows a large variation in the between the shear rates and is the model that fits the experimental value least. The Matijašić model was best for one value, but based on the overall results, one can say that the Chhabra model is the best model.

3.3 Conclusions

As a result of the first feasibility test, it was decided to use five of the particles in the experiment. 0.001 m, 0.002 m, 0.003 m, 0.004 m and 0.015 m were chosen because these particles were heavy enough for the weight to obtain the exact value and thus having the opportunity to calculate the density. The two smallest particles were not used because they were too light, and the weight was not able to determine the value due to poor resolution.

In the second feasibility test it was shown that the chosen concentrations of PAC were suitable for the experiment. The flow of the particles was possible to define and the velocities were also obtained. It was shown, similar to water, that the particle with the smallest diameter had the lowest velocity and the particle with the biggest diameter had the highest velocity. There was also observed that the particles moving in a cluster had a higher velocity combined than a single particle alone.

The quality of the photos was good, so it was not necessary to confirm the events with the high-speed camera. Since the results were satisfying, it was decided that it was not necessary to do the experiment with PAC in the cell. Instead, it was decided to do an experiment with an oil-water system in the graduated cylinder.

Regarding the comparison between experimental and theoretical results, it was shown that none of the models were particularly good and gave deviating results. This shows that one must be critical of which model and rheology values to use. Overall, the Chhabra model using the shear rate of 1 s^{-1} was the most suitable.

Chapter 4

Experimental setup

4.1 Mechanical construction

A small-scale cell intended for this project was already built, but had not been used before. The cell consisted of four glass walls, reinforced with an aluminum frame, placed on a circular base, also of aluminum. The aluminum sections were made by Ryfylke Aluminium. The cell had the following measurements: height: 1.52 m, lenght: 0.100 m, width: 0.0500 m, diameter of base: 0.328 m. An illustration of the cell, including measurements, can be seen in Figure 4.1. The cell had some leaks, and these were sealed by silicon glue. Several components were added to the cell to simplify the conduct of the experiments. These were also modified and optimized several times due to new solutions being developed along the way.

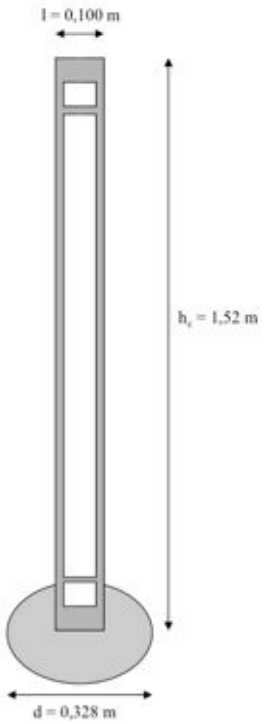

Figure 4.1: Small-scale cell

A particle collector was one of the components being added to the cell. This was needed because the particles had to be removed from the bottom of the cell after they had been dropped, as they would interfere with further particles if they remained in the cell. At first, there was made a collector of steel with a nylon stocking around it, attached to fishing thread. The idea was to lower the collector to the bottom of the cell and hoist it up again every time a particle needed to be removed. This turned out to be a poor solution, so another particle collector was developed.

The next idea for a particle collector was to place a funnel inside, at the bottom of the cell. Measurements were taken and a model of the funnel was made of cardboard, to serve as a template for the actual funnel that was going to be made of acryl. Pieces of acrylic plates were cut out; the end pieces were bent using a heat gun, and then all the pieces were glued together.

Afterwards, a 0.018 m hole was drilled through the base and frame of the cell, so the particles could flow through. The acrylic funnel was then set, covering the hole, so that the funnel would collect and guide the particles trough the bottom hole. In the hole underneath the base there was set a pipe nipple, which was attached to a hose with a valve. The valve was set to control the flow of fluid and to be able to clear out the particles. For the pipe nipple, there was used thread tape to protect the threads and to seal better. There was also set a gasket between the bottom of the cell and the base to prevent leakage through the hole.

The cell was finally placed on top of a stand 0.4 m above the ground, so it would be easier to reach underneath when the particles needed to be removed. This was the final solution regarding the particle collector and was used during the experiments. An Figure of the funnel with its measurements is presented in Figure 4.2.

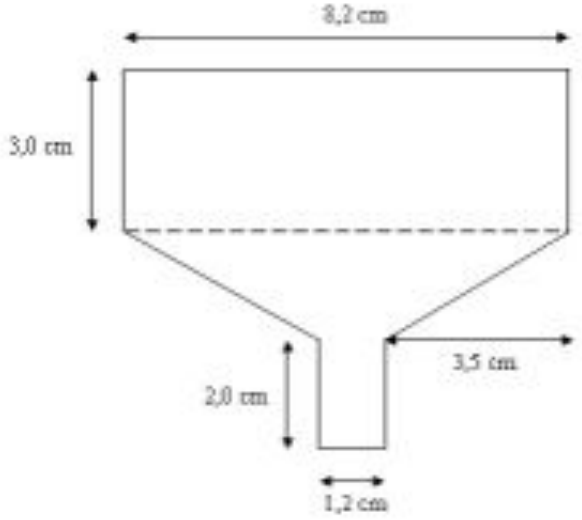

Figure 4.2: Funnel

An inner wall was the other component being added to the cell. There was need for an inner wall because of the risk of upward flow interfering with the downward flow. The inner wall was going to be placed close to one of the sides and not going entirely down to the bottom, letting the upward flow go on the inside of the wall and the downward flow go on the outside of the wall, not interfering with each other.

Several different solutions were tried as to what could be used as an inner wall. At first, a piece of plastic cardboard was cut out and tried placed in the cell. It was not stiff enough and got bent as it was forced further down the cell. Secondly, skirting was found and thought to be suitable. It was not wide enough, so adhesive rubber was put along one side to make it wider. The skirting was then tried to place into the cell, but the same problem occurred here; it was not stable enough and kept falling to one side as it was forced further down the cell. A larger piece of acryl was then tested. This was thicker, which would imply that it was more stable. This was not wide enough either, so adhesive rubber was put along both sides to make it wider. This solution worked to some extent, but still it was not optimal.

It was decided to use an acrylic pipe as the next solution. The pipe was 1,47 m long with a diameter of 0.024 m. It was set into the cell, attached with magnets. There were set two magnets inside the pipe, one at the bottom and one at the top. These magnets were attached with double-sided tape. Then there was placed two magnets on the outside of the glass wall, one at the top and one at the bottom. These magnets attracted the magnets inside the pipe and held it in place. This was the final solution regarding the inner wall and was used during the first experiments.

Based on the first results, it was decided to remove the inner wall from its place. It was assumed that the particles are so small that the inner wall has no effect. Instead, it was decided to place the pipe in the center of the cell and drop the particles through the pipe. From the previous experiments it was seen that the particles tended to go towards one side of the cell, which made the quality of the photos poor. It was desirable that the particles would fall in the center, which was possible now as they were dropped through the pipe. The pipe was cut to a shorter length, 0,894 m, and was centralized at two places in the cell. It was centralized at the bottom by steel wire, and at the top it was centralized by arms attached to the facilities behind the cell. The particles were then dropped trough the pipe and the photos were taken when the particles passed the end of the pipe and continued further down in the cell. A model of the setup with measurements is shown in Figure 4.3.

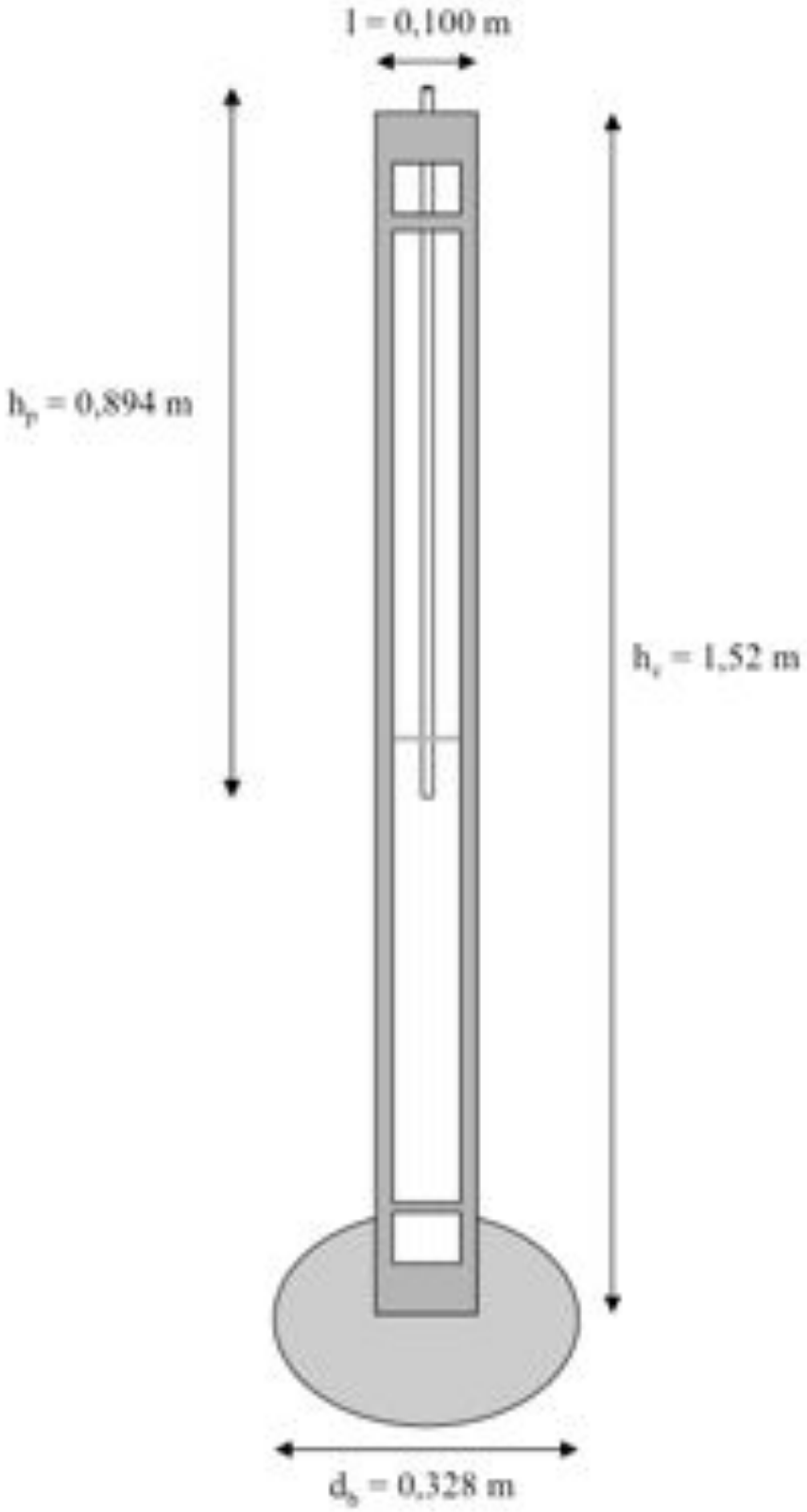

Figure 4.3: Final setup; cell with inner pipe

4.2 PIV

Particle Image Velocimetry (PIV) was used to complement the video recordings for the water-experiments done in the cell. Grilltex 2A seeding particles from EMS Griltech were added to the water in order to visualize the movement of the flow, thus revealing its velocity profile. The seeding particles are neautral buoyant particles with a density of 1.05 g/cm^3, and a size of 63-80 μm. In order to make the seeding particles visible, a laser was used to illuminate the flow. The flow was then recorded and the data was analyzed. Further details regarding visualization equipment and data processing can be found later in chapter 4.5 and 4.6, respectively. An illustration of seeding particles illuminated by a laser can be seen in Figure 4.4.

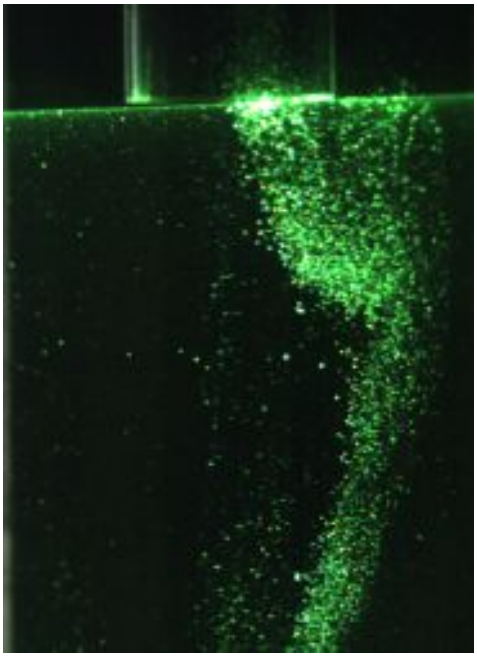

Figure 4.4: PIV seeding particles

4.3 Two-phase system

Instead of doing the experiments with PAC in the cell, it was decided to look at an oil-water system in the graduated cylinder. This was desirable to study because many drilling fluids are a mixture of oil and water and it would be interesting to see the behavior of the particles in a two-phase system. PAC was used as the water-based solution and Bayol 35 was used as the oil-based solution. 0.8 l of PAC-4g/l was remained in the cylinder, and 0.2 l of Bayol 35 oil was added on top. The 0.003 m glass beads were used and studied both in single and cluster movements. An illustration of the oil-water system can be seen in Figure 4.5 (a).

There was also done a study on an oil-water-gas system. This case would be applicable if there was influx of gas, e.g. a gas kick, in the well. The gas was created by shaking the cylinder and create air bubbles. The 0.003 m glass beads and the

0.004 steel spheres were used in this system and were studied in cluster movements. An illustration of the oil-water-gas system can be seen in Figure 4.5 (b). These experiments were only done with PAC-4g/l and was recored both by the Samsung camera and the high-speed camera.

(a) Oil-water system (b) Oil-water-gas system

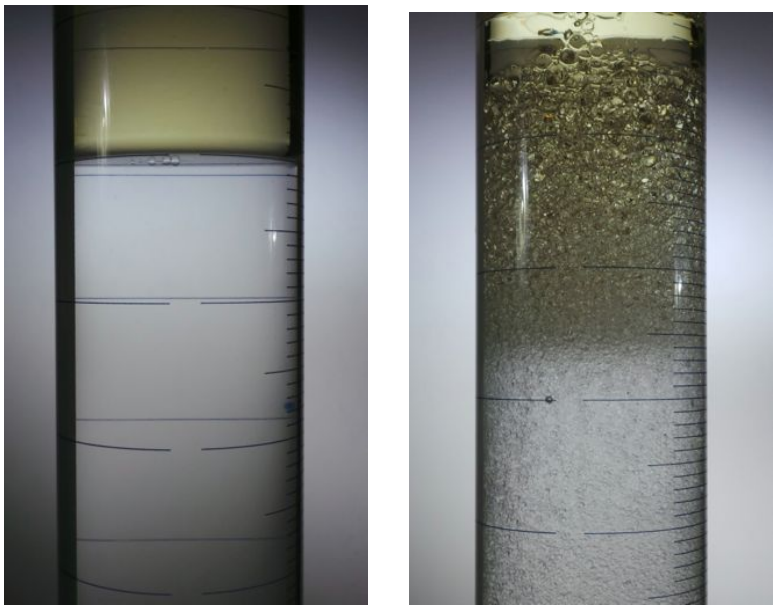

Figure 4.5: Oil-water/oil-water-gas system

4.4 Fluid rheology and density

Three different fluids were used in this thesis; water, PAC-4g/l and PAC-8g/l. The non-Newtonian fluids PAC-4g/l and PAC-8g/l were used because it was desirable to see how the particles would behave in fluids with higher viscosities than water.

The Polyanionic Cellulose (PAC) was mixed in a Silverson L2R laboratory mixer emulsifier with a Square Hole High Shear Screen workhead, as shown in Figure 4.6. The cell had a volume of 4,2 l, but there was made 6 l in case of spill. PAC-4g/l was mixed by dissolving 24 g of PAC into 6 l of water. PAC was added slowly to the water to avoid flocculation. The mixer had variable speed settings. This was not specified in rpm, but in levels from 1 to 10, where level 10 was maximum speed. PAC-4g/l was mixed at level 5 in the beginning and at level 8 in the end. PAC-8g/l was mixed in the same manner, except with a higher concentration of PAC. 48 g of PAC was added to 6 l of water. The mixture of PAC-8g/l was more viscous than the mixture of PAC-4g/l, so it had to be mixed at maximum speed.

The decision stating that it was not necessary to do the experiments with PAC in the cell was taken after these mixtures were made. On the basis of that, these mixtures of PAC were not used.

Figure 4.6: Silverson L2R laboratory mixer emulsifier

To measure the viscosity of the fluids, a rotation rheometer from Anton Paar was used. The equipment consisted of a MCR 302 viscometer and a CP50-1 cone plate configuration. A part of the equipment is shown in Figure 4.7. To exert forces, a cone plate configuration was rotated in contact with the fluid. The diameter of the cone was 49.972 mm and the angle of the cone to the test plate was set to 0.982°. To determine the rheology of the fluid, the shear rate was set to decrease from 1020 s^{-1} to 1 s^{-1} and then increase back to 1020 s^{-1}. This was done to check if the fluid, due to influences from the rheometer, gave deviation or hysteresis. The rheometer took 16 measuring points in 10 seconds for every shear rate. The fluid was kept constant at 20°C with automatic temperature control from the rheometer [5]. The rheology measurements were done before the experiment because it was assumed that the forces exerted by the experiment would not affect the rheology of the fluid.

To measure the mass density of the fluids, a density meter of the type Anton Paar DMA 4500 was used. This was a fully automated system that only required that one set a specific temperature and then injected the fluid into the apparatus. The temperature was set to 20.0 °C and 2 ml of fluid was injected. Approximately 1 minute later, the density was determined and shown on the screen of the apparatus, as in Figure 4.8. As with the rheology measurements, the density measurements were done before the experiment.

Figure 4.7: Anton Paar MCR 302 rheometer [5]

Figure 4.8: Anton Paar DMA 4500 density meter [2]

4.5 High-speed recording and visualization equipment

The visual part of the experiment was to record the particles with a camera to be able to obtain photos for the data processing later. There was used two cameras; a regular camera and a high-speed camera. The regular camera was of the type Samsung Galaxy EK-GC100 and has a capacity of 120 fps at a resolution of 768x720. The high-speed camera was of the type Speedcam MiniVis e2 from Weinberger,

which is a very light-sensitive high-speed camera. The camera enables high-speed recordings with a capacity of 2500 fps at full resolution (512x512). Together with the high-speed camera there was used a Photop Suwtech DPGL-2200L laser to visualize the PIV particles in the fluid. The laser has a wavelength of 532 nm and an output power of 200 mW [11]. To provide better lighting, two Labino white light lamps of the model H135 Midlight were used. The lamps provided a luminous flux of 3500 lm and the distribution angle was approximately 20° [12].

4.6 Data processing

After the recordings were done, the data had to be processed and the programs used were Avidemux, Matlab and the Matlab toolboxes PIVlab and MatPIV.

Avidemux is a free and open-source editing program designed for video editing and processing. It is written in C++ and uses either GTK+ or Qt for its userface [13]. Avidemux was used to process the photos taken by the Samsung camera. The camera recorded a slow-motion film with 120 fps, but did not split the frames. Also, the experiment was recorded with the camera in a vertical position to obtain a larger viewpoint. In Avidemux the film was rotated, cropped and split into frames.

Photos taken with both cameras were analyzed in PIVlab, which is a time-resolved digital PIV tool for Matlab. It is an open-source software that calculates the velocity distribution within image pairs and can also derive, display and export multiple parameters of the flow pattern. A suitable amount of photos recorded during the experiment were uploaded to PIVlab as image pairs. A region of interest was chosen and the interrogation area was adjusted to achieve smooth curves. The images were then analyzed. After the analysis was done, the units were converted from pixels per image-pair to m/s by doing a calibration, which meant selecting a reference distance and then entering the real distance [14]. As mentioned, PIVlab can display multiple parameters of the flow pattern, and vorticity was one of the parameters being studied closer.

The photos from the high-speed recording were analyzed in MatPIV, which is another PIV tool made to run with Matlab. It is similar to PIVlab, but MatPIV only look at one image pair at a time, meaning the actual analysis is done quicker. The Matlab program "PIV analysis spheres" was made to run with MatPIV, and the program displayed several parameters such as absolute velocity, velocities in annulus cross-section, vorticity etc.

Matlab was also used to find a theoretical velocity for the particles. The program "Kulefall Newtonian" is valid for Newtonian fluids and is based on formulas from the book "Multiphase Flows with Droplets and Particles" [3]. Parameters of the particle and fluid, such as particle diameter and density of both particle and fluid, were inserted and the terminal velocity was then calculated.

There was made a similar program "Kulefall non-Newtonian" for non-Newtonian fluids, which is based on Power law formulas by Chabra and Matijasic. n and K values from the rheology measurements were inserted and the program displayed several relations like path of particle, velocity components, drag coefficient vs. Reynolds number etc.

The Matlab scripts were made by Professor Rune W. Time and can be found in Appendix B.

Chapter 5

Results and discussion

5.1 Fluid rheology and density

Results from the rheology measurements for PAC-4g/l and PAC-8g/l can be found in Figure 5.1 and 5.2, respectively. The data series from the measurements can be found in Appendix A. The measurements were done twice, for both concentrations, to ensure that the results were correct. The results were virtually identical so only the first measurement is included.

The figures show two relations, viscosity vs. shear rate and shear rate vs. shear stress. Viscosity is displayed on the primary y-axis and is given in cP. Shear rate is shown on the x-axis and is given in 1/s. Shear stress is displayed on the secondary y-axis and is given in Pa. From the viscosity vs. shear rate relation it is clear that the fluid is shear thinning, as the viscosity decreases with an increasing shear rate. The shear stress increases as the shear rate increases. This applies to both PAC-4g/l and PAC-8g/l. The shear-thinning effect is a common property of polymer solutions and is consistent with the theory of PAC.

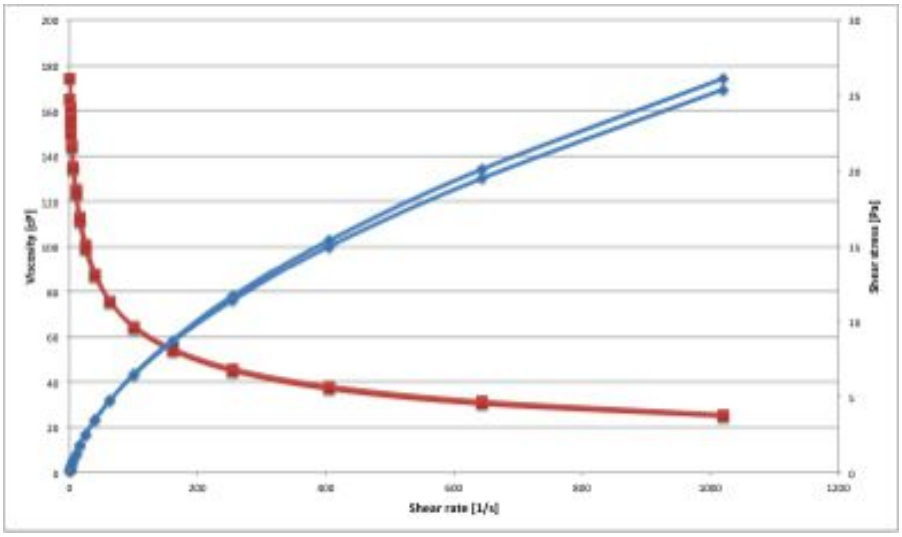

Figure 5.1: Rheology measurements for PAC-4g/l

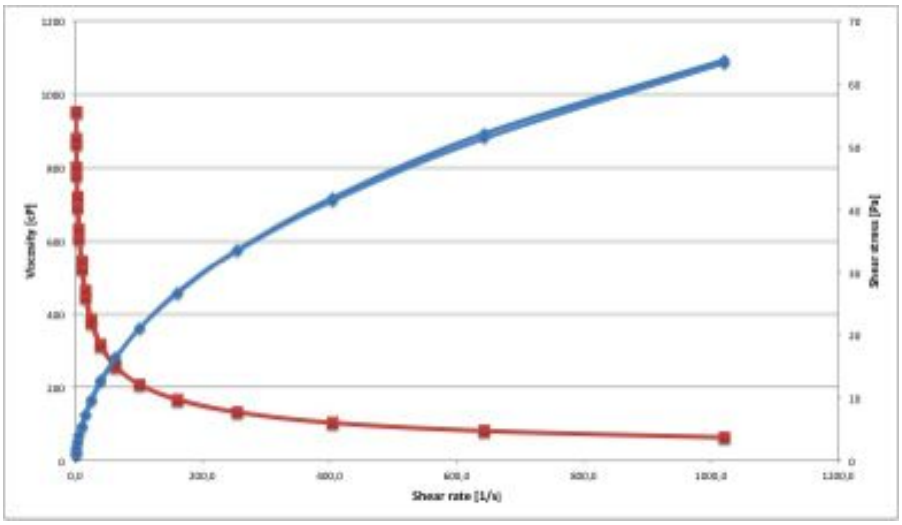

Figure 5.2: Rheology measurements for PAC-8g/l

Regarding differences between PAC-4g/l and PAC-8g/l one can see that PAC-8g/l is distinctly more viscous than PAC-4g/l. PAC-4g/l has a peak viscosity of 174 cP whereas PAC-8g/l has a five-time higher viscosity of 953 cP. The difference is not so big regarding the shear stress, but PAC-8g/l still has a peak shear stress of 63.8 Pa compared to PAC-4g/l with its shear stress of 26.1 Pa. These differences in the viscous properties are the main reason why the movements and velocities of the particles are so different in each fluid. It has been shown previously in the feasibility tests that the velocities decrease with an increasing viscosity. Also, the flow of the fluid went from dilute flow in water to dense flow in PAC.

When these rheology measurements were done, the shear rate was set to decrease from 1020 s^{-1} to 1 s^{-1} and then increase back to 1020 s^{-1}. This was done to check if the fluid, due to influences from the rheometer, gave deviation or hysteresis. From Figure 5.1 for PAC-4g/l one can see that there is hysteresis. Hysteresis is a physical phenomenon where the state changes as a result of external influences, but does not disappear when the influence is removed. It will only disappear after a reverse-oriented influence has worked with certain strength. The hysteresis can be seen by the gap between the two curves in the shear rate vs. shear stress relation. In Figure 5.2 for PAC-8g/l there is no gap between these two curves and hence there is no hysteresis.

The density measurements for the various fluids can be found in Table 5.1. One can see that PAC-4g/l is more dense than water, and PAC-8g/l is more dense than PAC-4g/l. This is consistent with the theory of PAC.

Table 5.1: Density measurements for water, PAC-4g/l and PAC-8g/l

	Water	PAC-4g/l	PAC-8g/l
Density $[kg/m^3]$	0.9983	0.9997	1.001
Specific gravity $[SG]$	1.001	1.002	1.003
Temperature [°C]	20.01	20.02	20.02

Rheology and density measurements of the Bayol 35 oil was not done, but the oil has been used and decribed before in a Bachelor's thesis by Nils Njå. The density was found to be 0.7922 kg/m^3 using the Anton Paar DMA 4500 densitymeter. The viscosity was found to be 1.030 cP using a Physica UDS 200 rheometer [15]

5.2 Terminal velocities in water

Here are the results from the water-experiments done in the cell. The particles used were the ones with a diameter of 0.001 m, 0.002 m, 0.003 m, 0.004 m and 0.015 m. Results from each particle is found here, and a summary can be found in Appendix A. The terminal velocity of the particles in water was calculated using the Matlab program "Kulefall Newtonian" and by looking at the pictures from the camera recordings.

The theoretical terminal velocity, $v_{t,t}$, was calculated in Matlab and is based on equations from the book "Multiphase Flow With Droplets and Particles" [3], which are previously described in chapter 2.3.

The experimental terminal velocity, $v_{t,e}$, is based on the camera recordings. It was considered the time spent for the particle to fall a certain height. An example of how the particle displacement is calculated is shown in Figure 5.3.

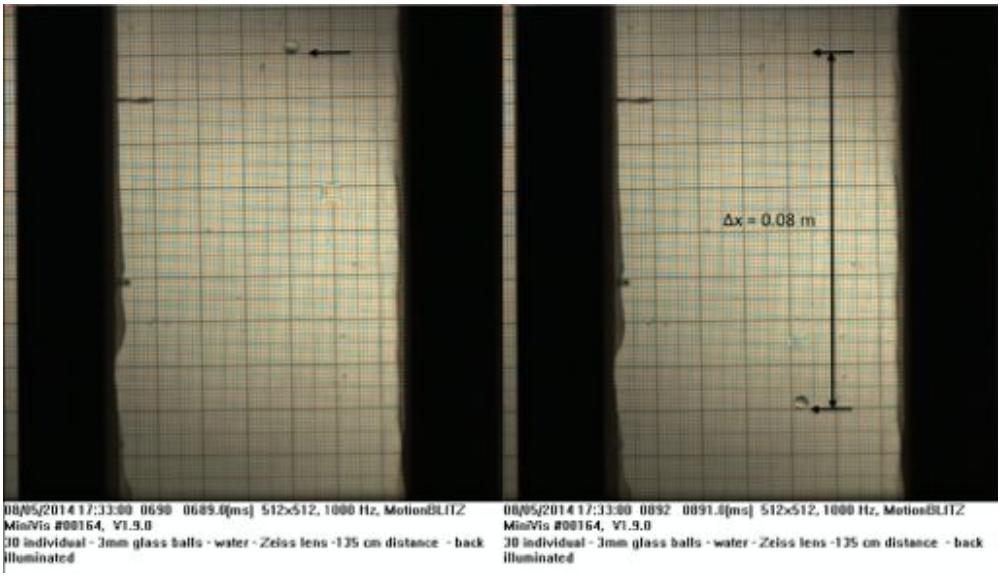

Figure 5.3: Scaling

There was used different methods for scaling. One method was taking a photo of a calibration scale before the recording, and then remove it. Another method was to place a graph paper behind the cell and keep it there throughout the experiment. The exact time for each frame was obtained either from Avidemux or from the high speed photos directly. The velocity was then calculated from the equation of motion

$$v_{t,e} = \frac{\triangle x}{\triangle t} \tag{5.1}$$

where $v_{t,t}$ is the terminal velocity, $\triangle x$ is particle displacement, $\triangle t$ is the time spent for the particle to drop the length of the scale.

5.2.1 0.001 m

From the Matlab program it was seen that the theoretical velocity for a particle with the diameter of 0.001 m was $v_{t,t,1} = 0.2254$ m/s. Figure 5.4 shows the velocity components of the particle and its terminal velocity. Velocity is displayed on the y-axis and is given in m/s. Time is shown on the x-axis and is given in seconds. One can see that the velocity in x-direction is zero and the particle reached its terminal velocity in the y-direction approximately after 0.1 seconds. The velocity is given as a negative value because the particle is going downward. This description of the plot also applies to the other velocity component plots obtained for the other particles, and is thus only described here.

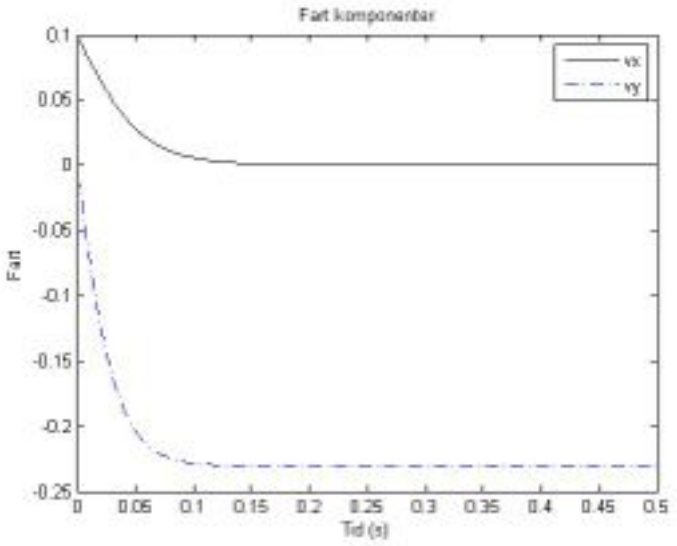

Figure 5.4: Velocity components of the 0.001 m particle

There were done several experimental attempts with the particle so the final velocity presented is an average of all the velocities obtained for this particle size. Experimental velocity of the particle with the diameter of 0.001 m was calculated to be $v_{t,e,1} = 0.1903$ m/s.

5.2.2 0.002 m

The theoretical velocity for a particle with a diameter of 0.002 m, calculated from the Matlab program, was seen to be $v_{t,t,2} = 0.2879$ m/s. Figure 5.5 shows the velocity components of the particle and its terminal velocity. It is seen that the particle reached its terminal velocity approximately after 0.15 seconds.

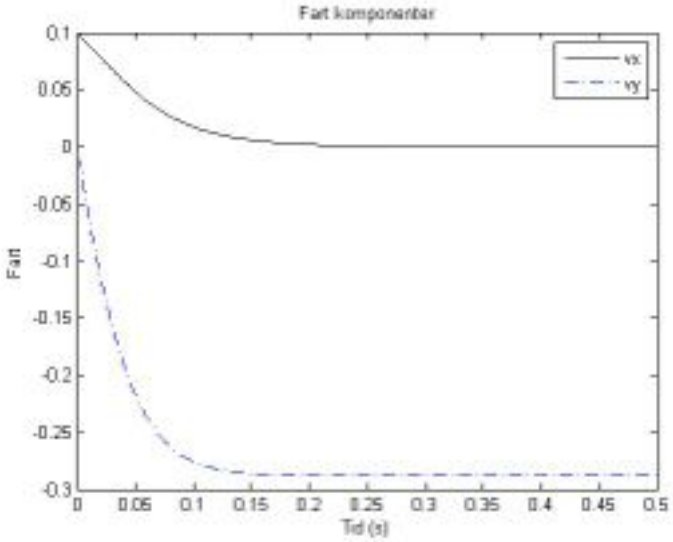

Figure 5.5: Velocity components of the 0.002 m particle

There were also done several experimental attempts with this particle size so the final velocity presented is also an average of all the velocities. Experimental velocity of the particle with the diameter of 0.002 m was calculated to be $v_{t,e,2} = 0.2828$ m/s.

5.2.3 0.003 m

From the Matlab program it was seen that the theoretical velocity for a single particle with the diameter of 0.003 m was $v_{t,t,3} = 0.3691$ m/s. The velocity components of the particle and its terminal velocity can be found in Figure 5.6. One can see that the particle reached its terminal velocity approximately after 0.2 seconds.

The 0.003 m particles were studied both in single and cluster movements and was recorded with the high-speed camera. The experimental velocity of a single particle with the diameter of 0.003 m was calculated to be $v_{t,e,3} = 0.3955$ m/s. Regarding the cluster of particles, the flow was considered to be dilute, as seen in Figure 5.7. Based on the results from the feasibility test, it was assumed that the velocity of the cluster was slightly higher than the velocity of a single particle, but this was not the case here. There was calculated several velocitites, depending on the placement in the cluster. Particles in the front, middle and back had a velocity of 0.3915 m/s, 0.3715 m/s and 0.3876 m/s, respectively, which is similar to the velocity for a single particle.

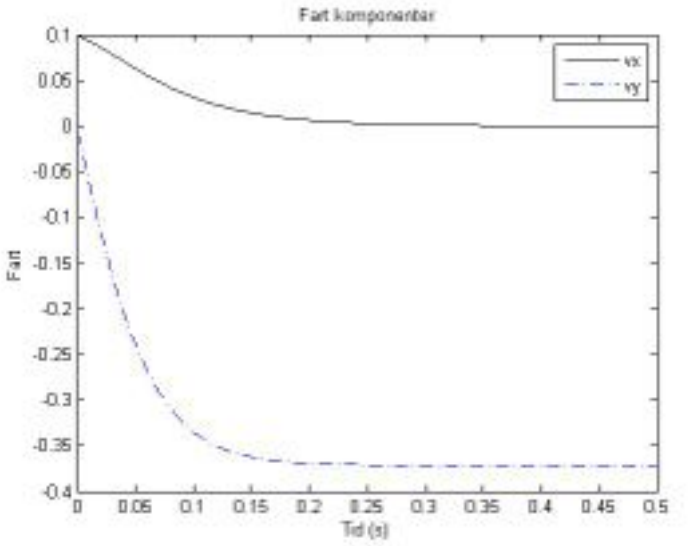

Figure 5.6: Velocity components of the 0.003 m particle

Figure 5.7: Cluster of 0.003 m glass beads

5.2.4 0.004 m

The theoretical velocity for a steel particle with the diameter of 0.004 m, calculated from the Matlab program, was seen to be $v_{t,t,4} = 0.9453$ m/s. The velocity components of the particle and its terminal velocity can be found in Figure 5.8. The terminal velocity of the particle was reached after approximately after 0.3 seconds.

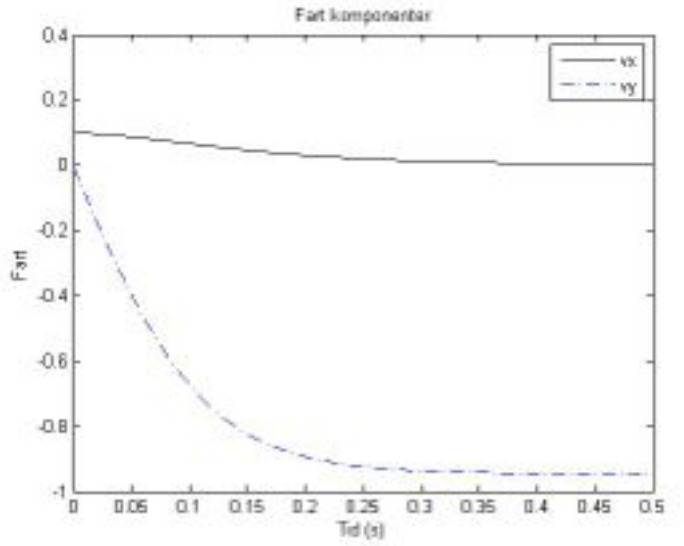

Figure 5.8: Velocity components of the 0.004 m particle

The 0.004 m particles were also recorded with the high-speed camera. The experimental velocity of the particle with the diameter of 0.004 m was calculated to be $v_{t,e,4}$ = 0.9872 m/s. In this experiment, there was observed an air bubble attached to some of the falling particles. This air bubble had a drag reduction effect on the particle and reduced the pressure differential of the rear and front. This effect increased the velocity of the particle and the larger the bubble, the higher velocity. The velocities with and without the air bubble can be found in Table 5.1. The 0.008 air bubble attached to the 0.004 steel sphere can be seen in Figure 5.9.

Table 5.2: Velocities for 0.004 m particle with air bubbles of various sizes

#	Lenght of air bubble $[m]$	Velocity $[m/s]$
1	0.000	0.9872
2	0.006	1.078
3	0.007	1.089
4	0.008	1.100

Figure 5.9: 0.004 m steel sphere with 0.008 m air bubble

5.2.5 0.015 m

From the Matlab program it was seen that the theoretical terminal velocity for a particle with the diameter of 0.015 m was $v_{t,t,15} = 1.665$ m/s. Figure 5.10 shows the velocity components of the particle and its terminal velocity. One can see that the particle reached its terminal velocity approximately after 0.5 seconds.

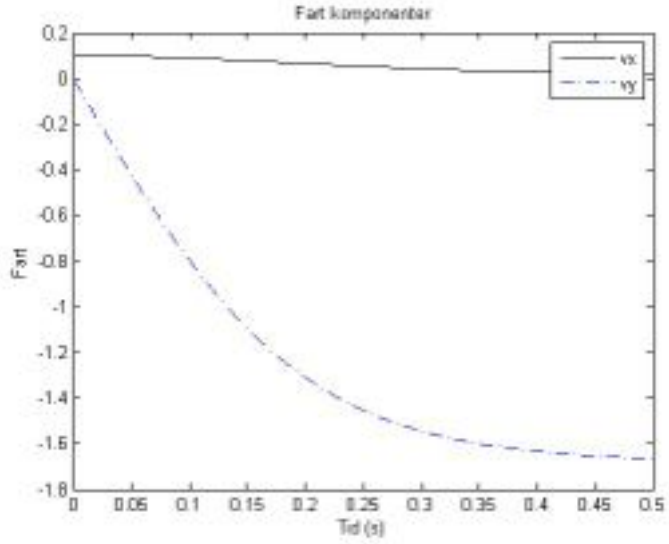

Figure 5.10: Velocity components of the 0.015 m particle

There were done several experimental attempts with the particle of this size. One was done without the inner pipe, and in this case the particle reached its terminal velocity rather quickly and the velocity was calculated to be $v_{t,e,15} = 0.1610$ m/s.

In the other experiments, the particle was dropped through the inner pipe. Since the inner diameter of the pipe was 0.024 m and not much larger than the diameter of the particle itself, the velocity of the particle was withheld when traveling through the pipe. It was not possible to calculate the terminal velocity due to the placement of the camera. It was placed too close to the cell and did not have a large enough viewpoint, so the highest velocity calculated from one of the recordings was 0.8320 m/s.

An interesting observation made in this case, was that this particle had a Taylor bubble attached to it when traveling through the pipe. The Taylor bubble split up when the particle passed the end of the pipe, but parts of the bubble stayed on while the particle traveled further down in the cell. It is assumed that this bubble gave the particle an increase in velocity as it did with the 0.004 m particle.

The particle with the Taylor bubble and its movements can be seen in Figure 5.11. In the first image, the particle is still inside the pipe and has the Taylor bubble attached to it. In the second image, the particle is on its way out of the pipe and the Taylor bubble is starting to break up. In the third image, the Taylor bubble is

about to break up and only a thin film is between the bubble and particle. In the fourth image, the bubble has broken up and the particle is traveling further down with parts of the bubble attached to it. The exact time for this sequence is given in each image frame.

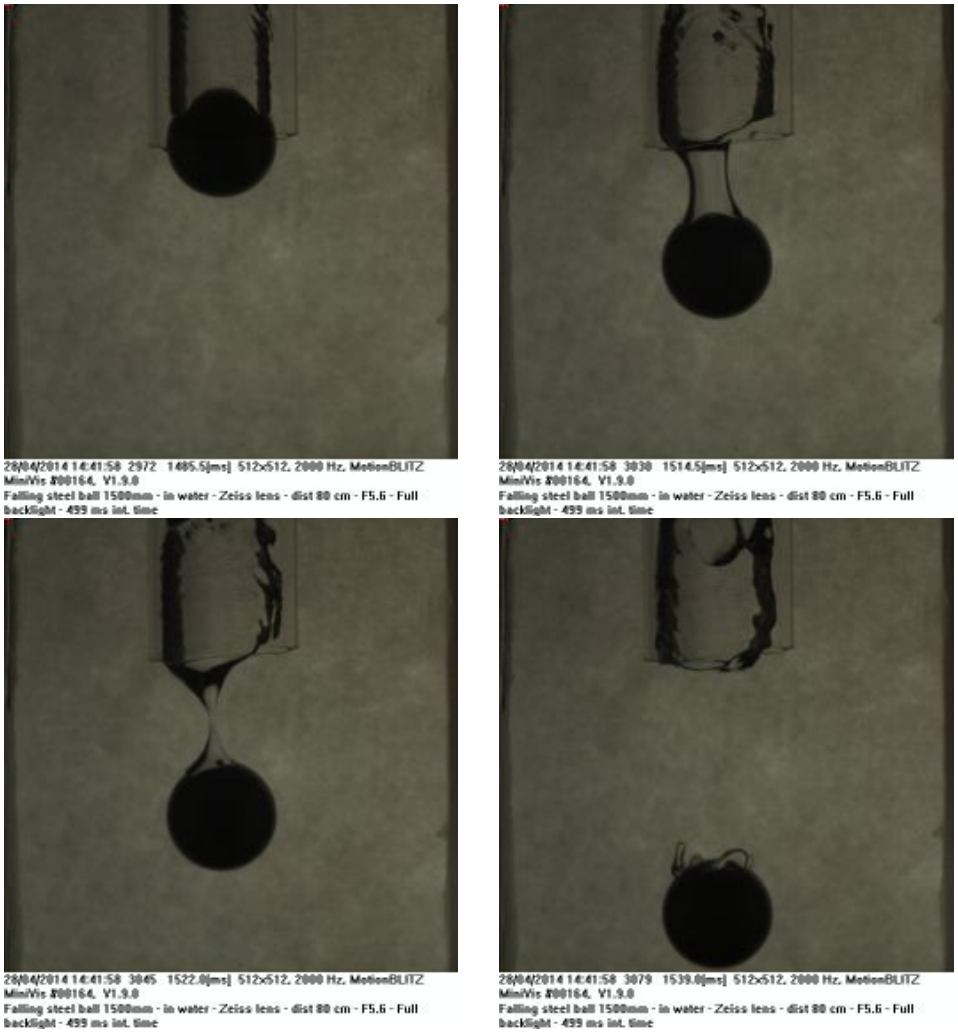

Figure 5.11: 0.015 m steel sphere with Taylor bubble

5.3 PIV

5.3.1 MatPIV

Here are the results from a PIV analysis done in MatPIV with a 0.004 m steel sphere. Figure 5.12 shows the image pair used for PIV correlations. Image 200 and 201 were used and the time between the frames were 1 ms.

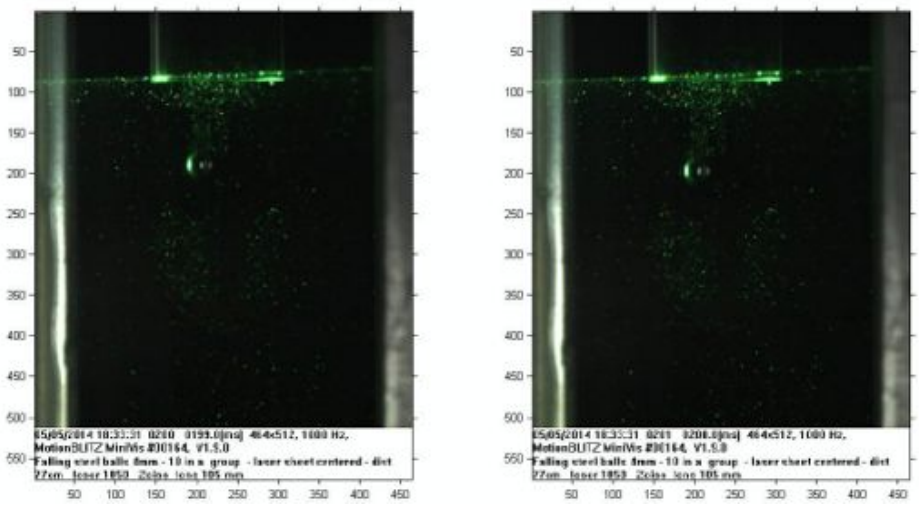

Figure 5.12: Image pair used for PIV correlations

Figure 5.13 is a plot showing the absolute velocity where the y-value is the vertical position in pixels and the x-value is the horizontal position in pixels. From the scale on the left, the absolute velocity can be found as approximately 0.9 m/s at some points. This is consistent with previous calculations.

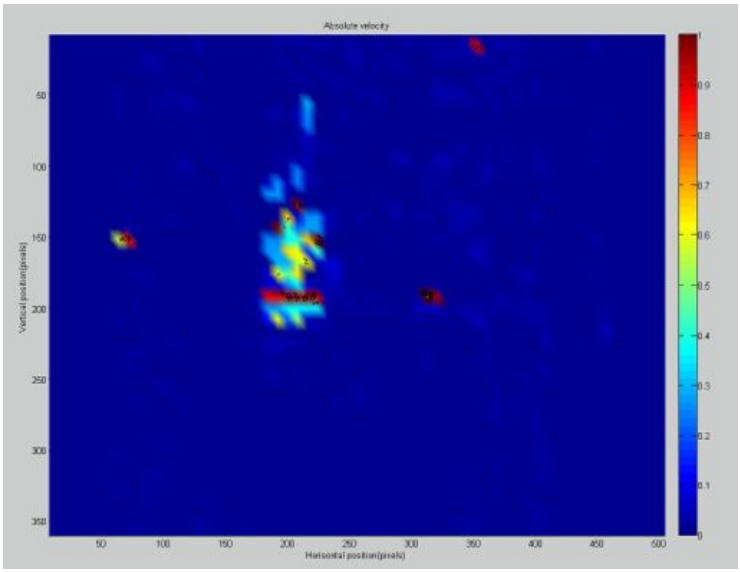

Figure 5.13: Absolute velocity

Figure 5.14 shows the vorticity of the particle. The y-axis shows the vertical position in pixels and the x-axis shows the horizontal position in pixels. The vorticity describes the flow of fluid around the particle. The blue area indicates a negative velocity, which in this case means that the fluid is moving along with the particle. Since the particle is moving downwards, the velocity is theoretically negative. The red areas indicate a positive velocity stating that the fluid is moving in a positive direction, but opposite relative to the particle.

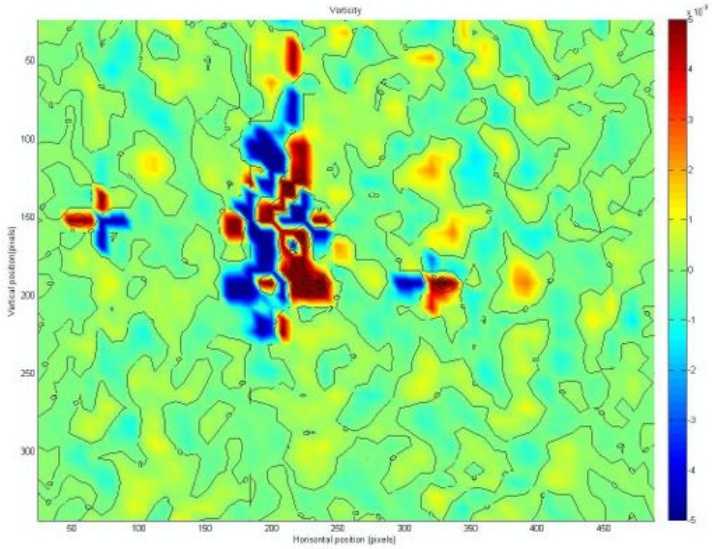

Figure 5.14: Vorticity

Figure 5.15 shows the velocity distribution from a vertical line along radial direction. The y-axis show the velocity given in m/s and the x-axis shows the horizontal position given in pixels. The cross section is taken at pixel 184, which approximately goes through the center of the particle. It can be seen that maximum velocity here is approximately 0.65 m/s. This deviates from the experimental velocity which was found to be 0.9872 m/s.

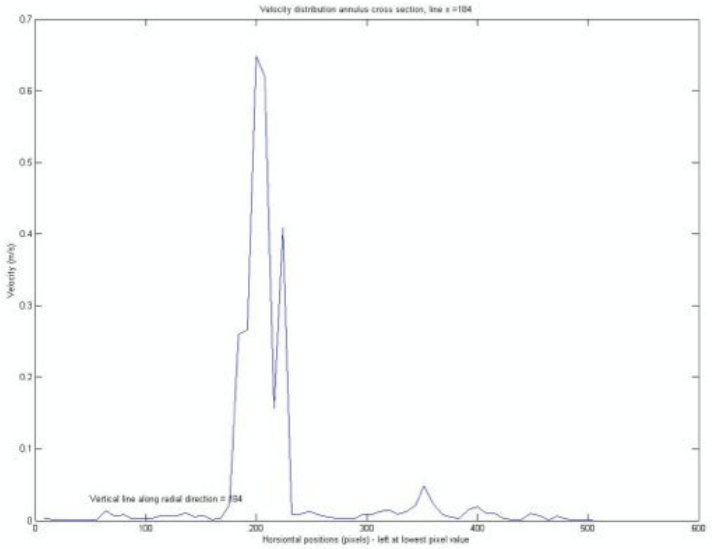

Figure 5.15: Velocity distribution

5.3.2 PIVlab

In PIVlab one had the option of uploading as many images as desirable. An attempt was made with 100 images, but the analyzed proved to take a very long time so it was decided to only analyze one image pair, thus two images. It was decided to analyze the same image pair in both PIVlab and MatPIV. This way, one could compare these results with the results from MatPIV.

Figure 5.16 is a quiver plot that displays velocity vectors as arrows with components (U,V) at the points (X,Y). One can see the vectors in front of the particle are pointing downwards, along with the flow. The vectors behind the particle are pointing upwards, also along with the flow.

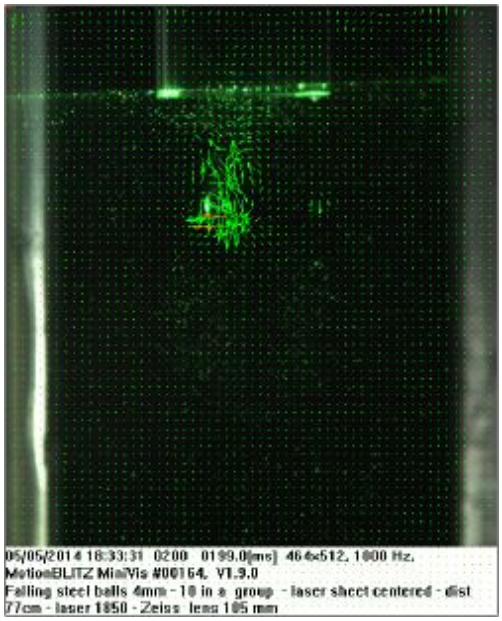

Figure 5.16: Velocity vectors

Figure 5.17 shows the velocity magnitude of the particle. From the scale, one can see that the maximum velocity is 0.7 m/s, which is a lower velocity than the one obtained from theory and experiments. The scale is given in the unit m/s. The vectors are also visible in this plot.

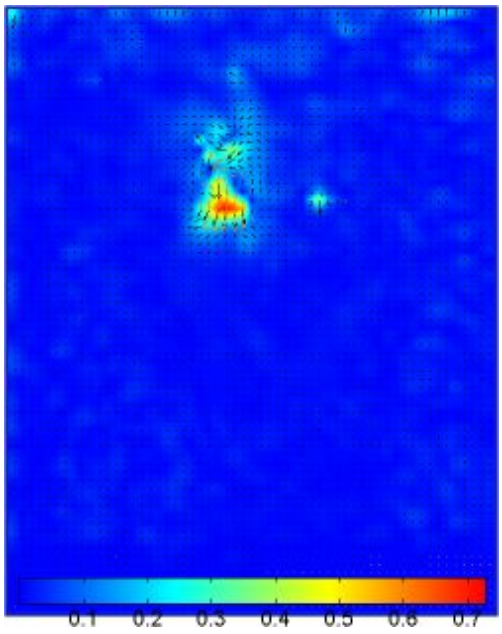

Figure 5.17: Velocity magnitude

Figure 5.18 shows the velocity magnitude of the particle along a cross sectional line. The parameters were extracted from a horizontal poly-line drawn through the center of the particle. The y-axis shows velocity magnitude and is given in m/s. The x-axis is showes the distance of the polyline given in meters. The figure shows a velocity of 0.7 m/s, which is lower than the velocity from theory and experiments, but it agrees with the velocity distribution obtained from MatPIV.

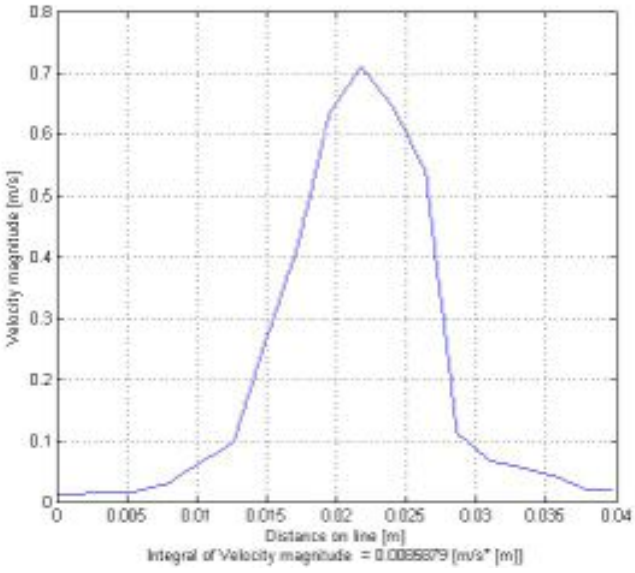

Figure 5.18: Velocity magnitude along a cross sectional line

Figure 5.19 shows the vorticity of the particle. This vorticity plot differ from the vorticity plot from MatPIV by being opposite relative to the particle. The blue area still indicates a negative velocity, but negative here means that flow is going in the opposite direction of the particle. The red area indicates a positive velocity, meaning the flow is going along with the particle. The unit of scale is in 1/s.

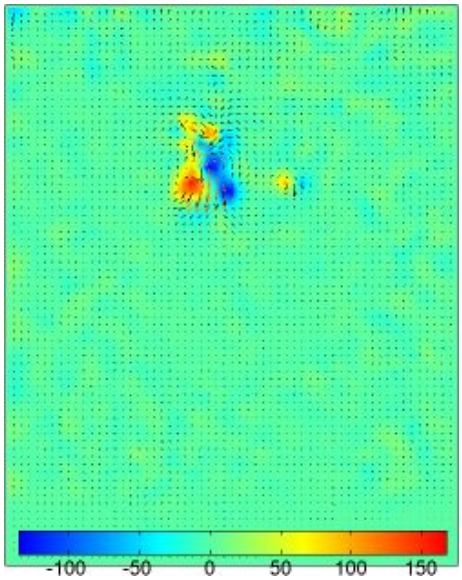

Figure 5.19: Vorticity

5.4 Two-phase system

5.4.1 Oil-water

The movement of the single 0.003 m glass bead in the oil-water system was studied first. The particle was released in the same manner as decribed in the feasibility test. After the particle was released, it spent 0.2 s before it reached the interface between oil and water, which gave it a velocity of 0.3421 m/s in the oil zone.

When it broke through the interface and traveled further down in the water zone, the particle brought along an oil droplet from the oil zone of approximately 0.002 m. This droplet was stretched as the particle traveled further, and eventually it burst into smaller parts. The movement of the particle from the oil zone to the water zone can be seen in Figure 5.20. In the first image, the particle is in the oil zone. In the second image, the particle is about to leave the interface, bringing along an oil droplet. In the third image, the particle is in the water zone with the oil droplet attached to it. In the fourth image, the oil droplet has split up into smaller parts. Some of continues further down with the particle and the rest of the droplet is started to rise back to the oil zone. The time sequence shown is set from when the particle hit the oil surface and the time spent for the particle to fall from then on.

(a) After 0.1325 s (b) After 0.2652 s (c) After 0.7875 s (d) After 2.022 s

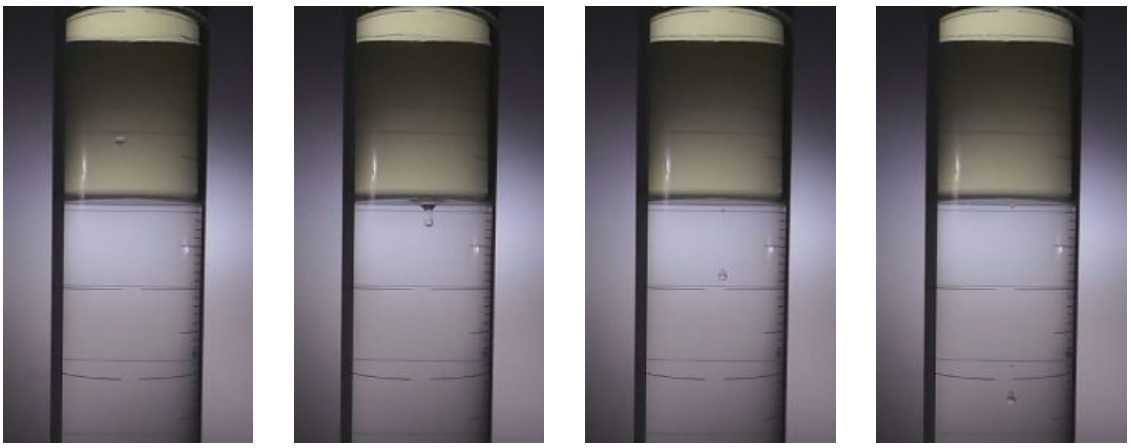

Figure 5.20: 0.003 m glass bead in oil-water system

The velocity obtained in the water zone was calculated to be 0.0420 m/s, which is slightly lower than the velocity in PAC-4g/l obtained from the feasibility test. From the experiments in water, the results showed that the velocity of a particle with an air-bubble would increase, and this was also the case here. Three other particles were studied, where the oil droplet was bigger, and these had a higher velocity of 0.0451 m/s, 0.0472 m/s and 0.0520 m/s.

Afterwards, several particles were released together in a cluster. During the oil zone, the particles acted as single particles and did not attract each other and the velocity was the same as the single particle, 0.3400 m/s.

When the particles broke the interface between oil and water, the velocity was decreased and they ended up in a dense cluster flow like previously shown in the feasibility test. Further down some of the particles fell out of the cluster, and some continued in the cluster. Since so many particles hit the interface at one time, they brought along a big film of oil, which eventually got thinner and slit up. Some of this film stayed with the remaining cluster and seemed to surround and hold the cluster together.

The movement of the particles can be seen in Figure 5.21. In the first image, the particles are released and some have already passes the oil zone, the interface and come into the water zone. In the second image, all of the particles have gotten into the water zone. The velocity is significantly decreased in the water zone so the last particles catches up with the first particles. One can see the large area of oil being brought into the water zone. In the third image, one can see the forming of the cluster and the oil film has become thinner. The instability in the interface is also observed. In the fourth image, some of the particles have fallen out of the cluster. One can see the oil droplet surrounding the cluster. The time sequence shown is set from when the particles hit the oil surface and the time spent for the particle to fall from then on.

(a) After 0.2915 s (b) After 0.4580 s (c) After 0.5830 s (d) After 0.8078 s

Figure 5.21: 0.003 m glass beads as a cluster in oil-water system

The velocity of the cluster in the water zone was calculated to be 0.1855 m/s. This is consistent with the result from the feasibility test where it was shown that clusters have higher velocity than a single particle.

5.4.2 Oil-water-gas

The 0.003 m glass beads and the 0.004 steel spheres were studied in the oil-water-gas system, and these experiments were recorded by the high-speed camera. Several 0.003 m particles were released at the same time and most them brought small air bubbles with them. These air bubbles split up before the particles reached the interface. The velocity obtained in the oil zone was found to be 0,5488 m/s. This is a higher velocity than the one obtained in the oil zone from the the oil-water system, so these small air bubbles might have given the particle an increase in velcocity.

It is observed that the particles spends a longer time to break through this interface. The interface in this case is an area of bubbles, so the exact interface between the oil zone and the water zone is not as clear as it was in the oil-water system. It is assumed that the particles must break through a film with surface tension, in addition to the viscous forces of the PAC. These forces combined will probably delay the flow of the particles in this particular area.

When the particles broke through the interface and got into the water zone, the velocity was decreased. It seems like the particles pulled oil into the water zone, but this broke up when the particles got further into the water zone. The velocity obtained in the water zone was found to be 0,0696 m/s. This velocity is also higher than the velocity obtained in the water zone from the oil-water sytem. Since this is the case for both the oil zone and water zone, it is assumed that the gas itself increases the velocity of the particles.

Figure 5.22 shows the movement of the 0.003 m particle in this system. The first image shows the particles in the oil zone. The second image shows the particles passing the interface and pulling the oil into the water zone. The third image shows the particles in the water zone. The oil went back to the oil zone when the particles broke out of the interface. The fourth image shows the particles further down in the water zone. One can see traces of the path the particles took when leaving the interface. The exact time for this sequence is given in each image frame.

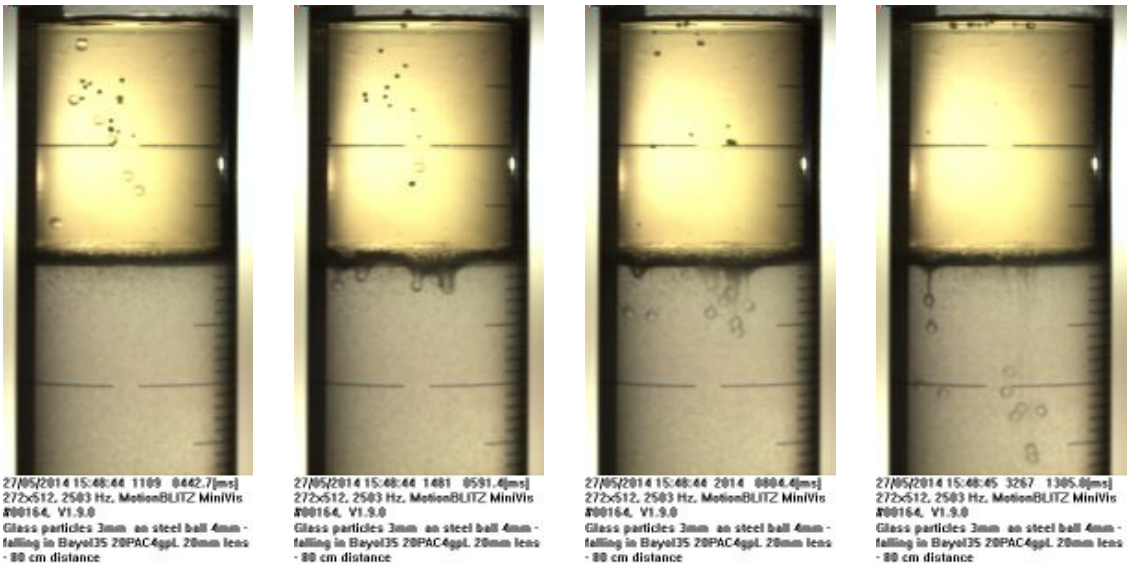

Figure 5.22: 0.004 m glass steel spheres in an oil-water-gas system

The 0.004 m steel spheres were released right after the 0.003 m glass beads. One particle was very interesting, as it had a very large air bubble along with it into the oil zone. The air bubble was approximately 0.017 m long. This bubble did not split up during the oil zone and followed the particle into the interface. The velocity obtained in the oil zone was found to be 1,207 m/s which is the highest velocity obtained for this particular particle. From previous result it was shown that the bigger air bubble, the higher velocity, so it is assumed that this very long air bubble contributed greatly to this high velocity.

As mentioned, the air bubble followed the particle into the interface. In Figure 5.23, photo nr. 2, one can see that the particle has gone through the interface and the bubble is still in the oil zone. Half of the air bubble stopped at the interface, but the rest stayed with the particle further down. It is unclear if the remaining bubble in the water zone is is air or oil, but it is observed that the bubble that was left at the interface rises faster than the bubble in the water zone, so it is assumed that the bubble in the water zone is oil.

Figure 5.23 shows the movement of the 0.004 m particle. In the first image, the particle has just entered the oil zone and one can the big air bubble attached to it. One can also see a particle that was released prior to this one. In the second image

one can the particle through the interface. The particle itself has passed and is on its way out, but the air bubble is on its way into the interface. In the third image som can see the breaking up of the bubble. In the fourth image one can see that the droplet has been split into smaller parts. Some is still attached to the particle and the rest is on its way up the oil zone. The exact time for this sequence is given in each image frame.

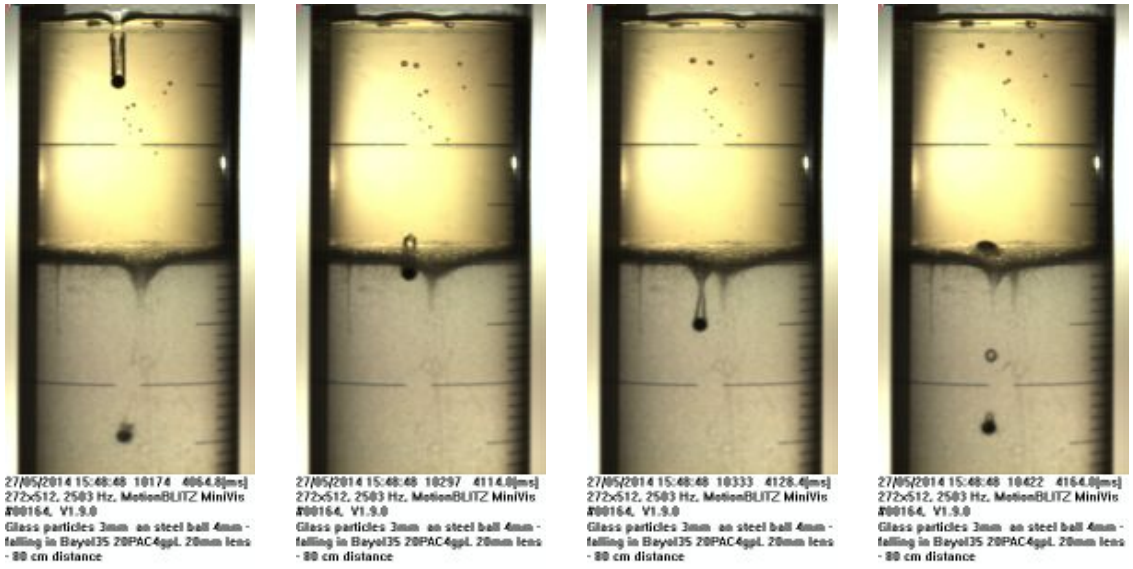

Figure 5.23: 0.004 m steel spheres in an oil-water-gas system

The velocity obtained in the water zone was found to be 1,015 m/s. There has not been done previous experiments with the 0.004 steel sphere in PAC, but since the velocity obtained here is not much different from the velocity obtained in water, there is reason to believe that these steel spheres are so heavy that they are not equally affected by the viscosity changes as the lighter particles.

Chapter 6

Conclusion

A large part of the task was to modify the setup. It was an intensive process with several challenges along the way, but with the many modifications done, the final result was satisfying. The funnel and the discharge system functioned as intended and the particles were easily cleared out of the cell. The function of the inner pipe served very well. When the particles were dropped inside the pipe, they kept falling in the middle of the cell. This generated good quality of the photos, where the particles were centered within the frame. There was one drawback with the pipe, but this only applied to the experiments done with the 0.015 m steel sphere. Since the diameter of the pipe was not much bigger than the diameter of the steel sphere, the velocity was withheld inside the pipe. This caused that the particle needed longer time to reach its terminal velocity.

Rheology and density measurements were done prior to the experiment. As from the theory, the polymer follow a shear-thinning, or pseudoplastic, behavior. The difference in density and viscosity for water and PAC caused the differences in flow behavior and velocity for the various particles. Increased viscosity provides a more viscous fluid, which can easily be seen in the movement of the particles. It was the increased viscosity in PAC that caused the decreasing of the velocity of the particles. The increased viscosity also changed the movement of the cluster-flow to go from dilute in water to dense in PAC.

The terminal velocity of the particles was determined with different methods. One method was theoretical and based on a Matlab program. The other method was experimental and based on the camera recordings. The terminal velocities obtained from the experiments with water in the cell are summarized the Table 6.1. How much the experimental velocity deviated from the theoretical velocity is also studied and given in percent. One can see that the velocities are fairly coherent. The 0.001 m particle has the highest value of deviation, but 15.56 % is an acceptable value.

Table 6.1: Summary of terminal velocities in water

d $[m]$	$v_{t,t}$ $[m/s]$	$v_{t,e}$ $[m/s]$	σ [%]
0.001	0.2254	0.1903	- 15.56
0.002	0.2879	0.2828	+ 1.740
0.003	0.3691	0.3955	+ 7.164
0.004	0.9453	0.9872	- 4.428
0.015	1.665	1.610	- 3.318

The PIV analyses were considered to successful. The results from MatPIV and PIVlab were similar, and the toolboxes are thought of as equally good as long as they are run with an equal number of image pairs. From MatPIV, the absolute velocity of the 0.004 m steel sphere in water was found to approximately 0.9 m/s. This agrees well with both the theoretical and experimental value. The vorticity showed the fluids movement around the falling particle. It was observed that the fluid was going in the opposite direction of the particle on one side, and in the same direction as the particle on the other side, which is the expected movement of the flow. The velocity distribution was studied in both MatPIV and PIVlab, in a vertical and horizontal direction, respectively. The line was drawn in the center of the particle in both directions. In the vertical direction, the maximum velocity was calculated to be 0.65 m/s. In the horizontal direction it was found to 0.7 m/s. These values correspond well with each other, but they are lower than the obtained velocity from theory and experiments.

In the two-phase system, the velocity findings from the second feasibility test with PAC were confirmed in the oil-water sytem. The velocities in PAC were similar to the ones in the feasibility test. It was also seen that the particles released in a cluster had a dense flow, compared to the dilute flow in water. The cluster also had a higher velocity than a single particle. The interesting thing found in this system is that when the particles went from the oil zone to the water zone it brought along droplets of oil. This droplet stayed with the particle as it traveled further down, but after a while it stretched and burst into smaller droplets and rose back towards the oil zone.

In the oil-water-gas system, the particles brought along air bubbles into the oil zone which gave an increase in velocity. It was also observed that the particles spent a longer time breaking through the interface, due to surface tension in addition to the viscous effect. The velocity in the water zone was also increased so it is assumed that the gas itself increased the velocity in both zones. The 0.004 m steel sphere brought a very long air bubble into the system and stayed with the particle through the oil zone and the interface. This resulted in a very high velocity. This agrees well with previous findings saying that the bigger the bubble is, the higher the velocity gets. The particle has a very high velocity in the water zone as well, similiar to the velocity obtained in water. Because of this, it is assumed that the steel spheres are so heavy that they are not equally affected by the viscosity changes as the lighter particles.

References

[1] M. Asyraf H. Al-Kayiem, N. Zaki and M. Elfeel. Simulation of the cuttings cleaning during drilling operations. *American Journal of Applied Sciences*, 2010.

[2] I. Verpe and M. Johnsen. Gas kick in vertical wells, an experimental study of gas kick, 2012.

[3] M. Sommerfeld C. Crowe, J. Schwarzkopf and Y. Tsuji. *Multiphase Flows with Droplets and Particles*. CRC Press, 2011.

[4] Dantec Dynamics. Measurement principles of piv. `http://www.dantecdynamics.com/measurement-principles-of-piv`, 16.06.14.

[5] K. Tjelta and I. Kvamme. Interfacial waves of taylor bubbles in vertical two-phase flow, 2013.

[6] L. Lake, editor. *Petroleum Engineering Handbook*, volume 1-7. Society of Petroleum Engineers, 2007.

[7] Universitetet i Stavanger. Øvinger i bore- og brønnvæsker, 2012.

[8] G. Matijasic and A. Glasnovic. Measurement and evaluation of drag coefficient for settling of spherical particles in pseudoplastic fluids. *ChemBioChem*, 2001.

[9] R.P Chhabra. *Bubbles, Drops, and Particles in Non-Newtonian Fluids*. CRC Taylor and Francis, 2nd edition, 2007.

[10] Dantec Dynamics. Particle image velocimetry. `http://www.dantecdynamics.com/particle-image-velocimetry`, 16.06.14.

[11] Photoptech. Photop suwtech laser datasheet. `http://www.photoptech.com`, 16.06.14.

[12] Labino AB. Labino compact white datasheet. `http://www.labino.com`, 16.06.14.

[13] Avidemux. `http://avidemux.sourceforge.net`, 16.06.14.

[14] Dipl. Biol. William Thielicke and Prof. Dr. Eize J. Stamhuis. Pivlab tutorial. `http://pivlab.blogspot.de/p/blog-page_19.html`, 16.06.14.

[15] N. Njå. Pressure drop and flow regimes with gas-liquid flow in horizontal pipelines, 2010.

Appendix A

Results

A.1 Feasibility test - Particles in microscope

Table A.1: Statistics of 0.001 m glass bead

#	Material	Diameter $[m]$	Weight $[kg]$	Volume $[m^3]$	Density $[kg/m^3]$
1	g	1.000E-03	2.100E-06	5.233E-10	4.013E+03
2	g	1.000E-03	2.200E-06	5.233E-10	4.204E+03
3	g	1.000E-03	2.200E-06	5.233E-10	4.204E+03
4	g	1.000E-03	2.200E-06	5.233E-10	4.204E+03
5	g	1.000E-03	2.100E-06	5.233E-10	4.103E+03
6	g	1.000E-03	2.200E-06	5.233E-10	4.204E+03
7	g	1.000E-03	2.100E-06	5.233E-10	4.013E+03
8	g	1.000E-03	2.100E-06	5.233E-10	4.013E+03
9	g	1.000E-03	2.100E-06	5.233E-10	4.013E+03
10	g	1.000E-03	2.200E-06	5.233E-10	4.204E+03

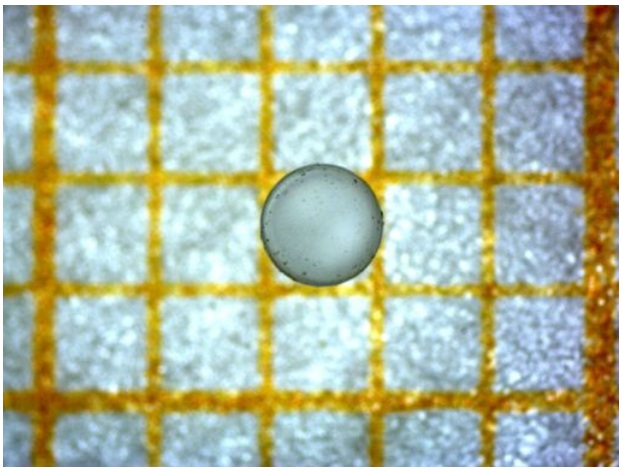

Figure A.1: 0.001 m glass bead in microscope

Table A.2: Statistics of 0.002 m glass bead

#	Material	Diameter $[m]$	Weight $[kg]$	Volume $[m^3]$	Density $[kg/m^3]$
1	g	2.000E-03	1.160E-05	4.187E-09	2.771E+03
2	g	2.000E-03	1.170E-05	4.187E-09	2.795E+03
3	g	2.000E-03	1.140E-05	4.187E-09	2.723E+03
4	g	2.000E-03	1.130E-05	4.187E-09	2.699E+03
5	g	2.000E-03	1.160E-05	4.187E-09	2.771E+03
6	g	2.000E-03	1.140E-05	4.187E-09	2.723E+03
7	g	2.000E-03	1.140E-05	4.187E-09	2.723E+03
8	g	2.000E-03	1.150E-05	4.187E-09	2.747E+03
9	g	2.000E-03	1.170E-05	4.187E-09	2.795E+03
10	g	2.000E-03	1.130E-05	4.187E-09	2.699E+03

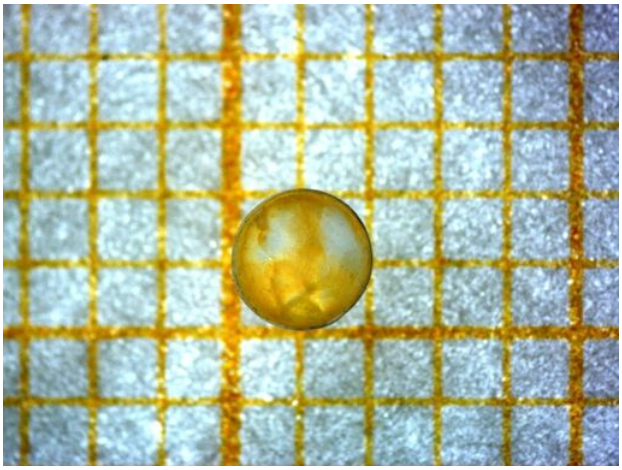

Figure A.2: 0.002 m glass bead in microscope

Table A.3: Statistics of 0.003 m glass bead

#	Material	Diameter $[m]$	Weight $[kg]$	Volume $[m^3]$	Density $[kg/m^3]$
1	g	3.000E-03	3.690E-05	1.413E-08	2.611E+03
2	g	3.000E-03	3.640E-05	1.413E-08	2.576E+03
3	g	3.000E-03	3.670E-05	1.413E-08	2.597E+03
4	g	3.000E-03	3.710E-05	1.413E-08	2.626E+03
5	g	3.000E-03	3.690E-05	1.413E-08	2.611E+03
6	g	3.000E-03	3.670E-05	1.413E-08	2.597E+03
7	g	3.000E-03	3.650E-05	1.413E-08	2.583E+03
8	g	3.000E-03	3.650E-05	1.413E-08	2.583E+03
9	g	3.000E-03	3.670E-05	1.413E-08	2.597E+03
10	g	3.000E-03	3.620E-05	1.413E-08	2.562E+03

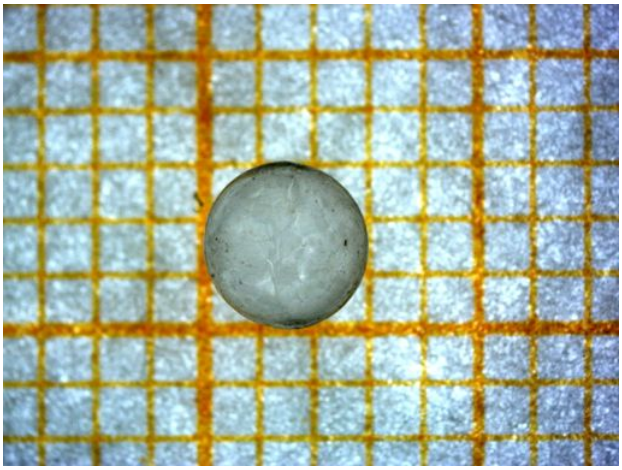

Figure A.3: 0.003 m glass bead in microscope

Table A.4: Statistics of 0.004 m steel sphere

#	Material	Diameter $[m]$	Weight $[kg]$	Volume $[m^3]$	Density $[kg/m^3]$
1	s	4.000E-03	2.534E-04	4.369E-08	7.566E+03
2	s	4.000E-03	2.531E-04	4.369E-08	7.557E+03
3	s	4.000E-03	2.537E-04	4.369E-08	7.575E+03
4	s	4.000E-03	2-537E-04	4.369E-08	7.575E+03
5	s	4.000E-03	2.532E-04	4.369E-08	7.560E+03
6	s	4.000E-03	2.534E-04	4.369E-08	7.566E+03
7	s	4.000E-03	2.535E-04	4.369E-08	7.569E+03
8	s	4.000E-03	2.536E-04	4.369E-08	7.572E+03
9	s	4.000E-03	2.535E-04	4.369E-08	7.569E+03
10	s	4.000E-03	2.536E-04	4.369E-08	7.572E+03

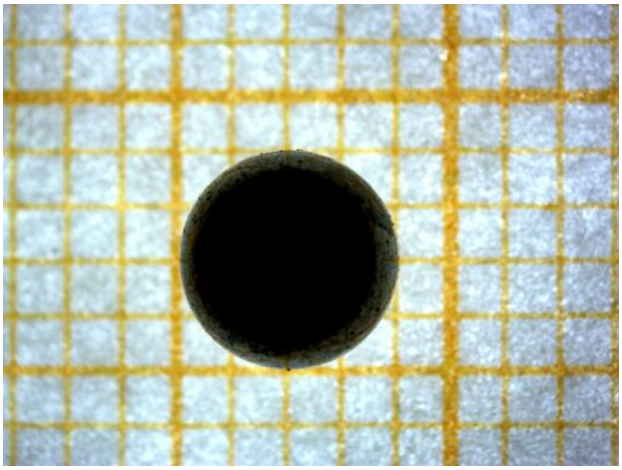

Figure A.4: 0.004 m steel sphere in microscope

A.2 Terminal velocities in water

Table A.5: Summary of terminal velocity with $\rho_w = 1000\ kg/m^3$ and $\mu_w = 0.001\ Pa * s$

#	Material	d $[m]$	$\rho_p\ [kg/m^3]$	$v_{t,e}\ [m/s]$	Re_e	$v_{t_t}\ [m/s]$	Re_t
1	g	1.000E-03	4.108E+03	1.903E-01	1.903E+02	2.254E-01	2.254E+02
2	g	2.000E-03	2.744E+03	2.828E-01	5.658E+02	2.879E-01	5.758E+02
3	g	3.000E-03	2.594E+03	3.955E-01	1.187E+03	3.691E-01	1.107E+03
4	s	4.000E-03	7.568E+03	9.872E-01	3.949E+03	9.453E-01	3.781E+03
5	s	1.500E-02	7.740E+03	1.610E-00	2.415E+04	1.665E+00	2.498E+04

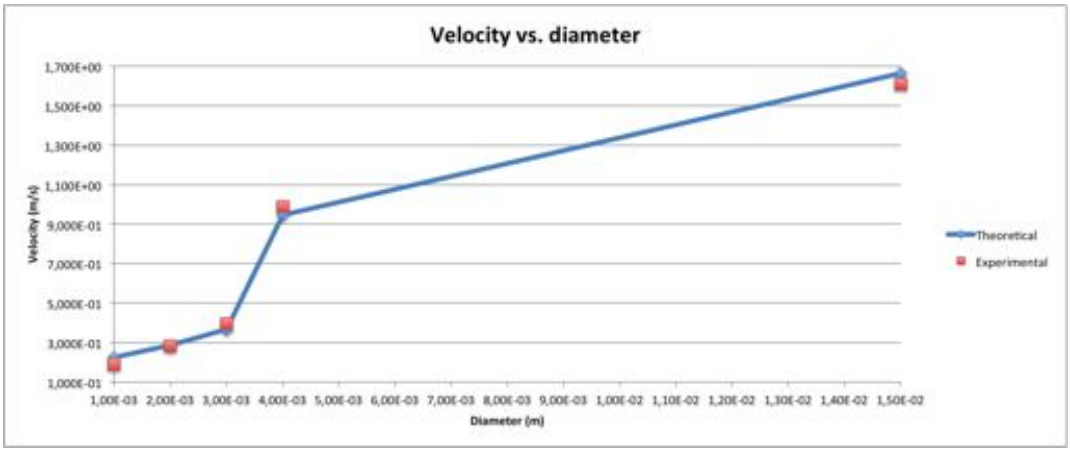

Figure A.5: Velocity vs. diameter

A.3 Fluid rheology

Table A.6: Viscosity measurements for PAC-4g/l

Shear rate $[1/s]$	Shear stress $[Pa]$	Viscosity $[cP]$
1020	26.1	25.6
643	20.1	31.3
405	15.4	38
255	11.7	45.7
161	8.78	54.6
101	6.54	64.5
63.8	4.8	75.3
40.2	3.49	86.8
25.4	2.51	98.9
16	1.77	111
10.1	1.24	123
6.34	0.848	134
4	0.58	145
2.52	0.377	150
1.59	0.244	154
1	0.174	174
1	0.165	165
1.59	0.256	161
2.52	0.395	157
4	0.577	144
6.34	0.858	135
10.1	1.26	125
16	1.81	113
25.4	2.55	101
40.2	3.54	87.9
63.8	4.82	75.5
101	6.48	64
161	8.66	53.8
255	11.4	44.8
405	15	36.9
643	19.5	30.3
1020	25.4	24.9

Table A.7: Viscosity measurements for PAC-8g/l

Shear rate $[1/s]$	Shear stress $[Pa]$	Viscosity $[cP]$
1020	63.8	62.6
643	52.1	81
405	41.9	103
255	33.6	132
161	26.8	167
101	21	207
63.8	16.3	255
40.2	12.5	310
25.4	9.45	373
16	7.08	443
10.1	5.24	520
6.34	3.83	604
4	2.76	690
2.52	1.96	777
1.59	1.37	863
1	0.95	950
1	0.953	953
1.59	1.4	882
2.52	2.02	803
4	2.88	720
6.34	4.02	633
10.1	5.5	547
16	7.41	464
25.4	9.81	387
40.2	12.8	317
63.8	16.4	257
101	21	207
161	26.6	165
255	33.4	131
405	41.4	102
643	51.3	79.9
1020	63.3	62.1

Appendix B

Matlab scripts

B.1 Kulefall Newtonian

```
% ***********************************************************
% Program for   beregne en kulepartikkels fall i et fluid
% ***********************************************************
% Baserer programmet p  boken "Multiphase flows with droplets
% and particles" (Crowe, Sommerfeld, Tsuji - 1998).
% Vi har benyttet lign. 2.24 for "Hastighets responstid"
% lign 4.53 for f (dragfaktor)
% og lign. 4.67 for akselerasjon
% ***********************************************************
% Enheter : SI  = m, kg, s
% ***********************************************************

% De tre neste kommadoene "rensker opp" i memory, figurer og utskriftsomrde
clear
clc
clf
% ******

% Definer tidspunkter og lag fast plass til s og v (posisjon og fart) vektorer
% ************************************************************************
N = 1000            % Antall tidsintervall
T = 0.5             % Total tidlengde
t=linspace(0,T,N);  % Lager en "tidsvektor" fra 0 til T med N elementer (N tidspunkt
dt = t(2)-t(1)      % Tidsintervall mellom hver tidspunkt

s = zeros(N,2);     % Posisjonsvektor ("lager") for hvert av de N tidsstegene.
                    % 2 angir at det er to komponenter pr. tidssteg
                    % dvs. x og y komponent
v = zeros(N,2);     % Hastighetsvektor ("lager") - som for posisjonsvektor

% Oppgi startverdier:
% *******************
s(1,:) = [ 0 0];        % Startposisjon  ( x og y koordinat)
v(1,:) = [ 0.100 0.614]; % Startfart

% DATA for vske og partikkel:
```

```
% ****************************
g  = [0  -9.81]              % Tyngdeakselerasjonsvektor  m/s^2
d  = 15000e-6                  % Partikkeldiameter
A  = pi*d^2/4                % Partikkeltverrsnitt
Vol = pi*d^3/6               % Partikkelvolum
rho_p = 7740                 % Partikkeltetthet kg/m^3
m = rho_p * Vol              % Partikkelmasse
rho_L = 1000                 % Vsketetthet
my_L  = 1e-3                 % Vskeviskositet (Pa*s)

% "Hastighets respons tid"  ved Stokes strmning
% ********************************************
t_v = rho_p*d^2/(18*my_L)    % Lign. 2.24

% Initialiser posisjon, hastighet og akselerasjon ved tidspunkt 1
% Det er besparende for program kjringen   lage et par sm vektorer vinst,
% sinst og aksinst som bare holder fortlpende verdier av fart, posisjon
% og akselerasjon. Vektorene v og s samler p  verdiene for alle tidspunktene.
% ********************************************************************
vinst = v(1,:)
sinst = s(1,:)
vabs = sqrt(vinst(1)^2+vinst(2)^2)     % Absoluttverdi av hastighet
Rer = rho_L*vabs*d/my_L;               % Reynoldstall

% Definer dragfaktor f = CD/(Rer*24) der CD er dragkoeffisient og Rer er
% Reynoldstall for partikkelen relativt omkringliggende vske (lign. 4.53)
f = 1 + 0.15*Rer^0.687 + 0.0175*Rer*(1 + 4.25e4*Rer^(-1.16))^(-1);

aksinst = (f/t_v)*(-vinst) + (1-rho_L/rho_p)*g     % "Instantan" akselerasjon
                                                   % basert p  lign 4.67

% Start tidslkke:
%*****************
for i = 1:N  % Lkke over tidssteg fra nr 2 og til siste tidssteg N
    sinst = sinst + vinst*dt + 0.5*aksinst*dt^2; % Oppdater posisjon
    vinst = vinst + aksinst*dt;                  % Oppdater fart
    v(i,:)= vinst;             % Kopier til "lager" vektor for fart
    s(i,:)= sinst;             % Kopier til "lager" vektor for posisjon
    vabs = sqrt(vinst(1)^2+vinst(2)^2);
    Rer = rho_L*vabs*d/my_L;    % Reynoldstall
    f = 1 + 0.15*Rer^0.687 + 0.0175*Rer*(1 + 4.25e4*Rer^(-1.16))^(-1);
    aksinst = (f/t_v)*(-vinst) + (1-rho_L/rho_p)*g; % Oppdater akselerasjon
end
% *** Slutt tidslkke ************

% Lag plott for posisjon (x-komp versus y-komp) for alle tidene
figure(1)
plot(s(:,1),s(:,2),'-.k')
title('Partikkelbane')
xlabel('x - koordinat ')
ylabel('y - koordinat ')

% Lag plott av x-komp og y-komp av partikkelhastigheten
figure(2)
plot(t,v(:,1),'-k')
hold on
```

```
plot(t,v(:,2),'-.b')

title('Fart komponenter')
xlabel('Tid (s)')
ylabel('Fart')
legend('vx','vy')
```

B.2 Kulefall non-Newtonian

```
% ************************************************************
% Program for   beregne en kulepartikkels fall i et fluid
% ************************************************************
% Baserer programmet p  boken "Multiphase flows with droplets
% and particles" (Crowe, Sommerfeld, Tsuji - 1998).
% Vi har benyttet lign. 2.24 for "Hastighets responstid"
% lign 4.53 for f (dragfaktor)
% og lign. 4.67 for akselerasjon
% ************************************************************
% Enheter : SI  = m, kg, s
% ************************************************************
% Andre gode referanser
% http://web2.clarkson.edu/projects/subramanian/ch301/notes/dragsphere.pdf
% ************************************************************

% De tre neste kommadoene "rensker opp" i memory, figurer og utskriftsomrde
clear all
clc
clf
format compact

% ******

% Definer tidspunkter og lag fast plass til s og v (posisjon og fart) vektorer
% ************************************************************************
N = 1000            % Antall tidsintervall
T = 0.2             % Total tidlengde
t=linspace(0,T,N);  % Lager en "tidsvektor" fra 0 til T med N elementer (N tidspunkt
dt = t(2)-t(1)      % Tidsintervall mellom hver tidspunkt

s = zeros(N,2);     % Posisjonsvektor ("lager") for hvert av de N tidsstegene.
                    % 2 angir at det er to komponenter pr. tidssteg
                    % dvs. x og y komponent
v = zeros(N,2);     % Hastighetsvektor ("lager") - som for posisjonsvektor

% Oppgi startverdier:
% *******************
s(1,:) = [ 0.12 0.0];        % Startposisjon  ( x og y koordinat)
v(1,:) = [ 0.0 0.0]; % [ 0.100 0.0]; % Startfart


% DATA for vske og partikkel:
% ***************************
g  = [0  -9.81]             % Tyngdeakselerasjonsvektor  m/s^2
% d  = 500e-6                 % Partikkeldiameter
```

```
d  = 30e-4                    % Partikkeldiameter
A  = pi*d^2/4                 % Partikkeltverrsnitt
Vol = pi*d^3/6                % Partikkelvolum
rho_p = 2600                  % Partikkeltetthet kg/m^3
m = rho_p * Vol               % Partikkelmasse
rho_L = 1000                  % Vsketetthet
my_L  = 1e-3                  % Vskeviskositet (Pa*s)

% "Hastighets respons tid"  ved Stokes strmning("relaksasjonstid" )
% ******************************************
t_v = rho_p*d^2/(18*my_L)    % Lign. 2.24

% Initialiser posisjon, hastighet og akselerasjon ved tidspunkt 1
% Det er besparende for program kjringen   lage et par sm vektorer vinst,
% sinst og aksinst som bare holder fortlpende verdier av fart, posisjon
% og akselerasjon. Vektorene v og s samler p  verdiene for alle tidspunktene.
% ***********************************************************************
vinst = v(1,:)
sinst = s(1,:)
vabs = sqrt(vinst(1)^2+vinst(2)^2)     % Absoluttverdi av hastighet
Rer = rho_L*vabs*d/my_L;               % Reynoldstall

% Definer dragfaktor f = CD/(Rer*24)FEIL!!!
% skal vre f= CD * Rer/24
% der CD er dragkoeffisient og Rer er
% Reynoldstall for partikkelen relativt omkringliggende vske (lign. 4.53)
f = 1 + 0.15*Rer^0.687 + 0.0175*Rer*(1 + 4.25e4*Rer^(-1.16))^(-1);

aksinst = (f/t_v)*(-vinst) + (1-rho_L/rho_p)*g      % "Instantan" akselerasjon
                                                    % basert p  lign 4.67

% Start tidslkke:
%*****************
for i = 1:N  % Lkke over tidssteg fra nr 2 og til siste tidssteg N
    sinst = sinst + vinst*dt + 0.5*aksinst*dt^2; % Oppdater posisjon
    vinst = vinst + aksinst*dt;                  % Oppdater fart
    v(i,:)= vinst;             % Kopier til "lager" vektor for fart
    s(i,:)= sinst;             % Kopier til "lager" vektor for posisjon
    vabs = sqrt(vinst(1)^2+vinst(2)^2);
    Rer = rho_L*vabs*d/my_L;    % Reynoldstall
    %    f = 1 + 0.15*Rer^0.687 + 0.0175*Rer*(1 + 4.25e4*Rer^(-1.16))^(-1);
    %Ny versjon fra Morrison - 2013
    Ledd1= (24/Rer);
    Rer5=Rer/5.0;
    Ledd2= (2.6*Rer5)/(1+Rer5^1.52);
    Rer263=Rer/263000;
    Ledd3=(0.411*Rer263^(-7.94))/(1+Rer263^-8);
    Ledd4=((Rer^0.8)/461000);
    CD =Ledd1+Ledd2+Ledd3+Ledd4;
    f=CD*Rer/24;
    RERI(i)=Rer;
    CDI(i)=CD;
    aksinst = (f/t_v)*(-vinst) + (1-rho_L/rho_p)*g; % Oppdater akselerasjon
end
% *** Slutt tidslkke ************
```

```
% Lag plott for posisjon (x-komp versus y-komp) for alle tidene
figure(1)
plot(s(:,1),s(:,2),'-.k')
title('Partikkelbane')
xlabel('x - koordinat ')
ylabel('y - koordinat ')

% Lag plott av x-komp og y-komp av partikkelhastigheten
figure(2)
plot(t,v(:,1),'-k')
hold on
plot(t,v(:,2),'-.b')

title('Fart komponenter')
xlabel('Tid (s)')
ylabel('Fart')
legend('vx','vy')


figure(10)
plot(t,RERI,'-k')

title('Reynoldstall vs time')
xlabel('Time (s)')
ylabel('Reynolds number')


figure(11)
plot(t,CDI,'-k')

title('CD vs time')
xlabel('Time (s)')
ylabel('CD')



Rlg= logspace(-2,7,1000);
Ledd1= (24./Rlg);
Rer5=Rlg/5.0;
Ledd2= (2.6*Rer5)./(1+Rer5.^1.52);
Rer263=Rlg/263000;
Ledd3=(0.411*Rer263.^(-7.94))./(1+Rer263.^-8);
Ledd4=((Rlg.^0.8)/461000);
CD = Ledd1+Ledd2+Ledd3+Ledd4;
flog = 1 + 0.15*Rlg.^0.687 + 0.0175*Rer*(1 + 4.25e4*Rer.^(-1.16)).^(-1);
CD2=24*flog./Rlg;
CD2=4*flog./Rlg;
figure(3)
loglog(Rlg,CD)
hold on
loglog(Rlg,CD2,'-r')
hold off



%NON-NEWTONIAN SETTLING (NN)
```

```
% Educated guess for powerlaw
K = 0.5
m =  K
n = 0.6


% **** Bruker Cchabra's  **********************
% RePL =rho_L* V^(2-n)*d^n/m (m er "consistency index") - lign 3.38 (s65)
% CD = (24/RePL)*(3^(2*n-3)*((n^2-n+3)/n^3*n) +
% ((4*n^4)/(24*(RePL)^((n-3)/3))
%RePL =rho_L* V^(2-n)*d^n/m
%CD = (24/RePL)*...
%    (3^(2*n-3)*((n^2-n+3)/n^3*n) + ((4*n^4)/(24*(RePL)^((n-3)/3))))

% Start fra v0 vertikalt
NNs = zeros(N,2);           % Posisjonsvektor ("lager") for hvert av de N tidsstegen
                            % 2 angir at det er to komponenter pr. tidssteg
                            % dvs. x og y komponent
NNv = zeros(N,2);           % Hastighetsvektor ("lager") - som for posisjonsvektor
NNs(1,:) = [ 0.12 0.0];     % Startposisjon  ( x og y koordinat)
NNv(1,:) = [ 0.0 1e-4];      % [ 0.100 0.0]; % Startfart

NNvinst = NNv(1,:);
NNsinst = NNs(1,:);
NNvabs = sqrt(NNvinst(1)^2+NNvinst(2)^2)        % Absoluttverdi av hastighet
RePL = rho_L*NNvabs^(2-n)*d^n/K                  % Reynoldstall for pseudoplastic
F1=3^(2*n-3)*((n^2-n+3)/n^(3*n));
F2=4*n^4/(24*(RePL)^((n-3)/3)) ;
NNCD=(24/RePL)*(F1+F2)


%
% Start IKKENWEWTONSK tidslkke:
%******************************
Vol=pi*d^3/6
Are=pi*d^2/4
m = Vol*rho_p
FG=g*(rho_p-rho_L)*Vol
Fgm= FG/m

FD = - NNCD*0.5*rho_L*NNvabs*NNvinst*Are
Fdm= FD/m
aksinst= Fdm + Fgm
%pause
for i = 2:N  % Lkke over tidssteg fra nr 2 og til siste tidssteg N
    i
    NNsinst = NNsinst + NNvinst*dt + 0.5*aksinst*dt^2;  % Oppdater posisjon
    NNvinst = NNvinst + aksinst*dt;                     % Oppdater fart
    NNv(i,:)= NNvinst;                  % Kopier til "lager" vektor for fart
    NNs(i,:)= NNsinst;                  % Kopier til "lager" vektor for posisjon
NNvabs = sqrt(NNvinst(1)^2+NNvinst(2)^2)        % Absoluttverdi av hastighet
RePL = rho_L*NNvabs^(2-n)*d^n/K                  % Reynoldstall for pseudoplastic
F1=3^(2*n-3)*((n^2-n+3)/n^(3*n));
F2=4*n^4/(24*RePL^((n-3)/3)) ;
NNCD=(24/RePL)*(F1+F2)
```

```
    FD = - NNCD*0.5*rho_L*NNvabs*NNvinst*Are
    Fdm=FD/m
    aksinst= Fdm + Fgm
    NRERI(i)=RePL;
    NCDI(i)=NNCD;
%    pause
end
% *** Slutt tidslkke ************

% Lag plott for posisjon (x-komp versus y-komp) for alle tidene
figure(15)
plot(NNs(:,1),NNs(:,2),'-.k')
title('Partikkelbane Powerlaw')
xlabel('x - koordinat ')
ylabel('y - koordinat ')

% Lag plott av x-komp og y-komp av partikkelhastigheten
figure(16)
plot(t,NNv(:,1),'-k')
hold on
plot(t,NNv(:,2),'-.b')

title('Fart komponenter Powerlaw')
xlabel('Tid (s)')
ylabel('Fart')
legend('NNvx','NNvy')

figure(17)
plot(NRERI,NCDI,'-k')

title('CD vs Powerlaw Reynoldstall')
xlabel('RePL')
ylabel('NCD')

% ****************************************************************
% **************Matijasic - 2001   Chem Biochem  *****************
% ****************************************************************
% Basert p  artikkel av Matijasic - 2001   Chem Biochem
% http://pierre.fkit.hr/hdki/cabeq/pdf/15_1_2001/Matijasic.pdf
% Konklusjon: CD = 24/RePS* A(n) + 0.653
% A(n) = -1.26*n + 2.3
% RePS = u^(2-n)*d^n*rho/K (K = Consistency index)
% Gjelder opp til RePS=1000
% An = -1.26*n + 2.3
% ****************************************************************

% Start fra v0 vertikalt
NNs = zeros(N,2);           % Posisjonsvektor ("lager") for hvert av de N tidsstegen
                            % 2 angir at det er to komponenter pr. tidssteg
                            % dvs. x og y komponent
NNv = zeros(N,2);           % Hastighetsvektor ("lager") - som for posisjonsvektor
NNs(1,:) = [ 0.12 0.0];     % Startposisjon  ( x og y koordinat)
NNv(1,:) = [ 0.0 1e-4];      % [ 0.100 0.0]; % Startfart

NNvinst = NNv(1,:);
NNsinst = NNs(1,:);
```

```
NNvabs = sqrt(NNvinst(1)^2+NNvinst(2)^2)        % Absoluttverdi av hastighet
RePL = rho_L*NNvabs^(2-n)*d^n/K                  % Reynoldstall for pseudoplastic
An = -1.26*n + 2.3
NNCD=An*(24/RePL)+0.653

%
% Start IKKENWEWTONSK tidslkke:
%******************************
Vol=pi*d^3/6
Are=pi*d^2/4
m = Vol*rho_p
FG=g*(rho_p-rho_L)*Vol
Fgm= FG/m

FD = - NNCD*0.5*rho_L*NNvabs*NNvinst*Are
Fdm= FD/m
aksinst= Fdm + Fgm
%pause
for i = 2:N  % Lkke over tidssteg fra nr 2 og til siste tidssteg N
    i
    NNsinst = NNsinst + NNvinst*dt + 0.5*aksinst*dt^2;  % Oppdater posisjon
    NNvinst = NNvinst + aksinst*dt;                     % Oppdater fart
    NNv(i,:)= NNvinst;                  % Kopier til "lager" vektor for fart
    NNs(i,:)= NNsinst;                  % Kopier til "lager" vektor for posisjon
NNvabs = sqrt(NNvinst(1)^2+NNvinst(2)^2)        % Absoluttverdi av hastighet
RePL = rho_L*NNvabs^(2-n)*d^n/K                  % Reynoldstall for pseudoplastic

NNCD=An*(24/RePL)+0.653

    FD = - NNCD*0.5*rho_L*NNvabs*NNvinst*Are
    Fdm=FD/m
    aksinst= Fdm + Fgm
    NRERI(i)=RePL;
    NCDI(i)=NNCD;
%    pause
end
% *** Slutt tidslkke ************

% Lag plott for posisjon (x-komp versus y-komp) for alle tidene
figure(25)
plot(NNs(:,1),NNs(:,2),'-.k')
title('Partikkelbane Powerlaw - Matijasic')
xlabel('x - koordinat ')
ylabel('y - koordinat ')

% Lag plott av x-komp og y-komp av partikkelhastigheten
figure(26)
plot(t,NNv(:,1),'-k')
hold on
plot(t,NNv(:,2),'-.b')

title('Fart komponenter Powerlaw - Matijasic')
xlabel('Tid (s)')
ylabel('Fart')
legend('NNvx','NNvy')
```

```
figure(27)
plot(NRERI,NCDI,'-k')

title('CD vs Powerlaw Reynoldstall- Matijasic')
xlabel('RePL')
ylabel('NCD')
```

B.3 PIV analysis spheres

```
% Program for PIV analyse av partikler
%*****************************************************
% Laget av:  Rune W Time 5 Mai - 2014
% Versjon 1 - tilpasset bilder fra mappen;
% "Falling 4mm steel balls - 10 in a group"
% *****************************************************
clc
cla
clf

iptsetpref('ImshowAxesVisible','on') % makes axes visible in "imshow"s

% Clip area of the full image
xclip1 = 1% 75%100;
xclip2 = 512%400;
yclip1 = 1;
yclip2 = 372  % 450% 512;

% Controls:
iles = 1    %Read picture file?
iberegn = 1 % New PIV calculation?
iplot = 1   % Draw plots?

nnstart=200   %First image to read
nnstop=nnstart    %Last image
dn=1        %Interleave factor

for i = nnstart:nnstop  %

    % Basic  stem of filename:
    im1=['Falling steel balls 4mm - 10 in a  group  - laser sheet centered - dist 77
lens 105 mm - no.'];
    % Convert picture numbers to a piece of text to enter the full file name;
    tall1=i+100000;
    tall2=i+dn+100000;
    ntall1=num2str(tall1);
    ntall2=num2str(tall2);

    %Construct the full filenames
    navn1=[im1 ntall1(2:6) '.bmp']
    navn2=[im1 ntall2(2:6) '.bmp']
    %J = i+1 %indekser fra 1 og oppover pga nn=0


    % ********** Reading sequence ***************
```

```
if iles==1 % iles settes verst i programmet
    bilde1 = navn1
    bilde2 = navn2

    [bilete, mappe] = imread(bilde1);
    utklipp1 = bilete(yclip1:yclip2, xclip1:xclip2);
    [bilete, mappe] = imread(bilde2);
    utklipp2 = bilete(yclip1:yclip2, xclip1:xclip2);

    figure(1)
    % clf(gca)
    subplot(1,2,1) % The two images used for PIV correlations in one
    imshow(bilde1)
    subplot(1,2,2)
    imshow(bilde2)
    hold on
    %axis([ 0 1000 0 2000 -1000 1000])
    axis('image')

    hold off

    % Store selected frames - temporarily
    % imwrite(utklipp1,'FrameA','tif')
    imwrite(utklipp1,'FrameA','bmp')
    % imshow(bilete)

    figure(2)
    imshow(utklipp2)
    hold on
    axis('image')
    %hold off
    % imwrite(utklipp2,'FrameB','tif')
    imwrite(utklipp2,'FrameB','bmp')

    figure(10)
    imshow(bilete)

    hold on
    xp = [xclip1 xclip2 xclip2 xclip1 xclip1]
    yp = [yclip1 yclip1 yclip2 yclip2 yclip1 ]
    plot(xp,yp,'-y') %draw the clpping area into the image
    hold off


end %end iles

%************   PIV calculation sequence   ***************
if iberegn==1  % iberegn=0 if no calculation
    sekvens = [64 64; 32 32; 16 16]; % interrogations areas

    %sekvens = [64 64; 32 32; 16 16; 8 8];
    %sekvens = 64;
    %sekvens = 32;
    dT = (dn)*1e-3; %Time between frame pairs
    [x,y,U,V,snr]= matpiv('FrameA','FrameB',sekvens,dT,0.5,'multi');
```

```
    % *********** Konvertering fra piksler til mm
    %
    % ********** Konvertering for gasslft ventilen  *****************
    % Mling med millimeterpapir 35mm svarer til piksel Y=329 nederst
    % og Y=36 verst. Dvs en piksel = 35 mm/(329-36) =35/293 =0.1195 mm
    % ***************************************************************
    %         Konvert=35/293;
    %         skalaP2C=293/35e-3;
    Konvert=0.024/(308-144); %meter per pixel
    skalaP2C=1/Konvert; % piksler per meter

    u = U/(skalaP2C);
    v = V/(skalaP2C);
    % SnR filter
    [su,sv]=snrfilt(x,y,u,v,snr,1.3);

end %end iberegn

Uabs = sqrt(u.^2 + v.^2); %Absolute velocity


% ********** Plotting sequence ************************
if iplot==1 % *********** iplot = 1
    % ************************************************
    figure(4)  % **********Quiver plott  **************
    imshow(utklipp1)
    hold on
    %axis([0 2200 0 2200])
    %       quiver(x,y,u,v,0.5,'-y');
    quiver(x,y,u,v,1,'-y');
    axis tight

    [C,h]=contour(x,y,Uabs)
    text_handle = clabel(C,h);
    set(text_handle,'BackgroundColor','n',... %[1 1 .6],...
        'Edgecolor','n')  % n =none 'w')  %[.7 .7 .7])
    hold off

    figure(5) %  ******  Uabs med fargekode -  som surf plott   *******
    surf(x,y,Uabs)
    hold on
    axis tight
    xlabel('Horisontal position(pixels)')
    ylabel('Vertical position(pixels)')
    title('Absolute velocity')
    % Color scale
    cmin = 0
    cmax= 0.3
    caxis([cmin cmax])
    shading interp
    view(0,-90) %view from above
    colorbar
    axis tight

    [C,h]=contour(x,y,Uabs)
    text_handle = clabel(C,h);
```

```
    set(text_handle,'BackgroundColor','n',... %[1 1 .6],...
        'Edgecolor','n')  % n =none 'w')  %[.7 .7 .7])
    hold off

    % [vty]= vorticity(x,y,u,v,'leastsq');
    % tur er laget fra vorticity pga konsistensproblemer med vorticity
    % turb=turbulens(x,y,u,v,'richardson');
    % turb=turbulens(x,y,u,v,'leastsq');
    turb=vorticity(x,y,u,v,'leastsq');

    figure(9)
    funn = find(turb<-0.4);
    turb(funn)=0;

    xa=x(3:end-2,3:end-2);
    ya=y(3:end-2,3:end-2);
    surf(xa,ya,turb)
    xlabel('Horisontal position (pixels)')
    ylabel('Vertical position(pixels)')
    title('Vorticity')

    % Color scale
    cmin = -5e-3
    cmax= 5e-3
    caxis([cmin cmax])
    shading interp
    view(0,-90)

    colorbar
    axis tight
    hold on
    [C,hturb]=contour(xa,ya,turb,'k')
    text_handle = clabel(C,hturb);
    set(text_handle,'BackgroundColor','n',... %[1 1 .6],...
        'Edgecolor','n')  % n =none 'w')  %[.7 .7 .7])
    line([184 184],[40 400],[0 0],'LineStyle','-','Color','k')
    hold off

end % end iplot ************************************
yadr = 20
horx =x(yadr,:);
abshast=Uabs(yadr,:);

figure(30)
plot(horx,abshast) %plot velocities in annulus cross section
title(['Velocity distribution annulus cross section, line x =' int2str(x(1,23))]
xlabel('Horsiontal positions (pixels) - left at lowest pixel value')
ylabel('Velocity (m/s)')
text(50,0.03,['Vertical line along radial direction = ' int2str(x(1,23))])

figure(2)
for jj=10:5:40
    abshast=Uabs(jj,:);
    yverdi=y(jj,1);
    plot(horx,yverdi,'.-k');
    plot(horx,yverdi+50*abshast,'.-b');
```

```
    end

    hold off
end %end nn
```

Appendix C

Illustrations

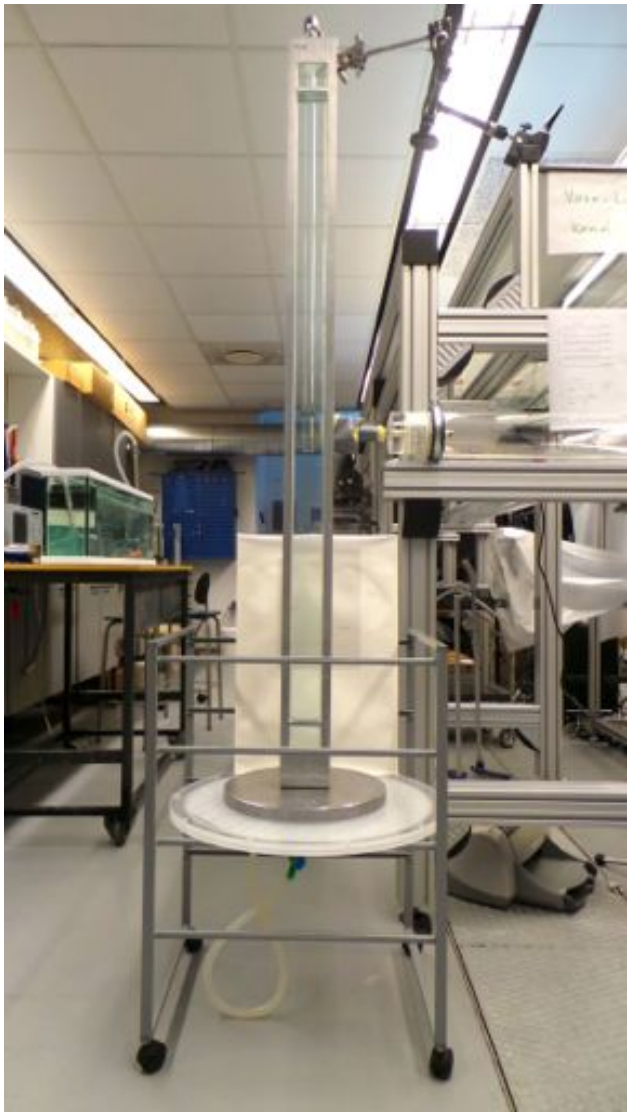

Figure C.1: Cell with complete setup

Figure C.2: Arms centralizing the inner pipe at the top

Figure C.3: Steel wire centralizing the inner pipe at the bottom

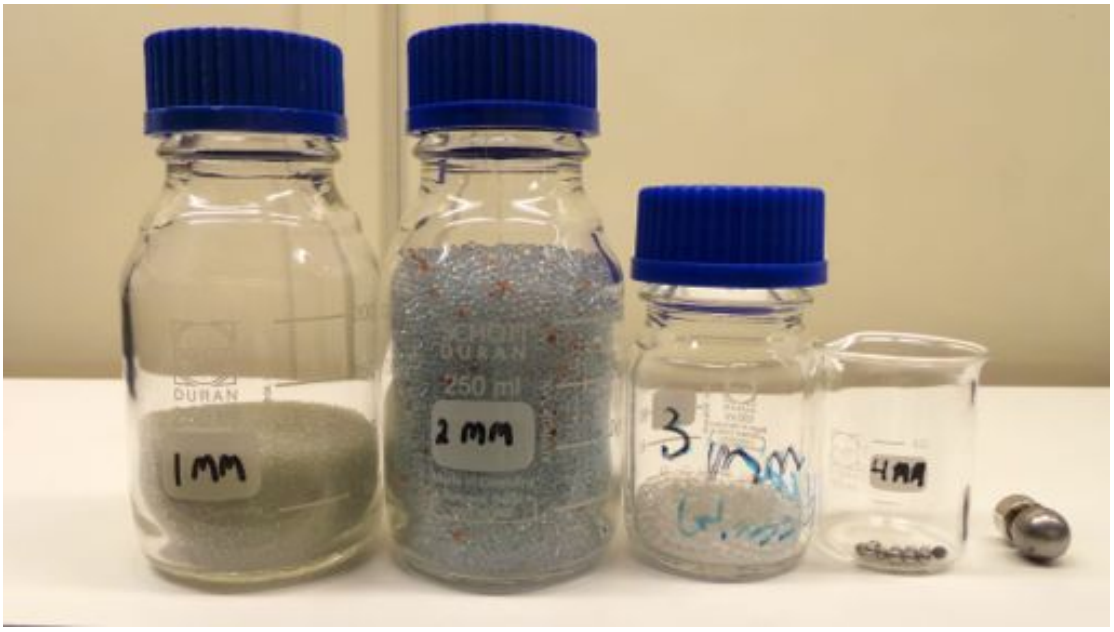

Figure C.4: Various particles

Figure C.5: Normet/Teknika microscope

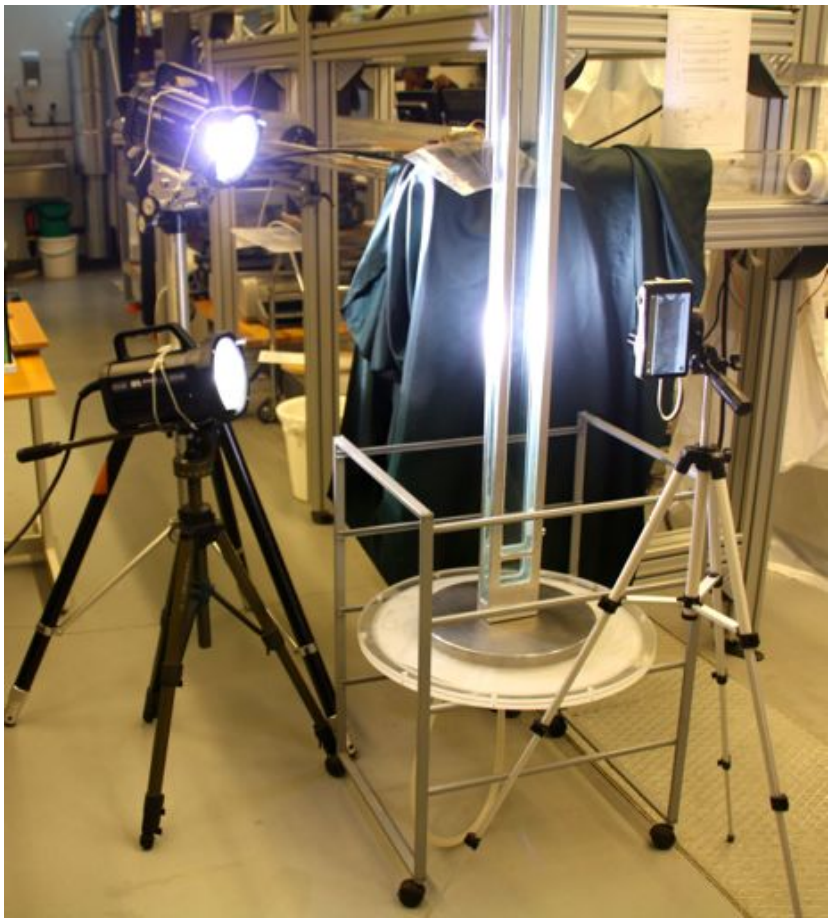

Figure C.6: Camera setup

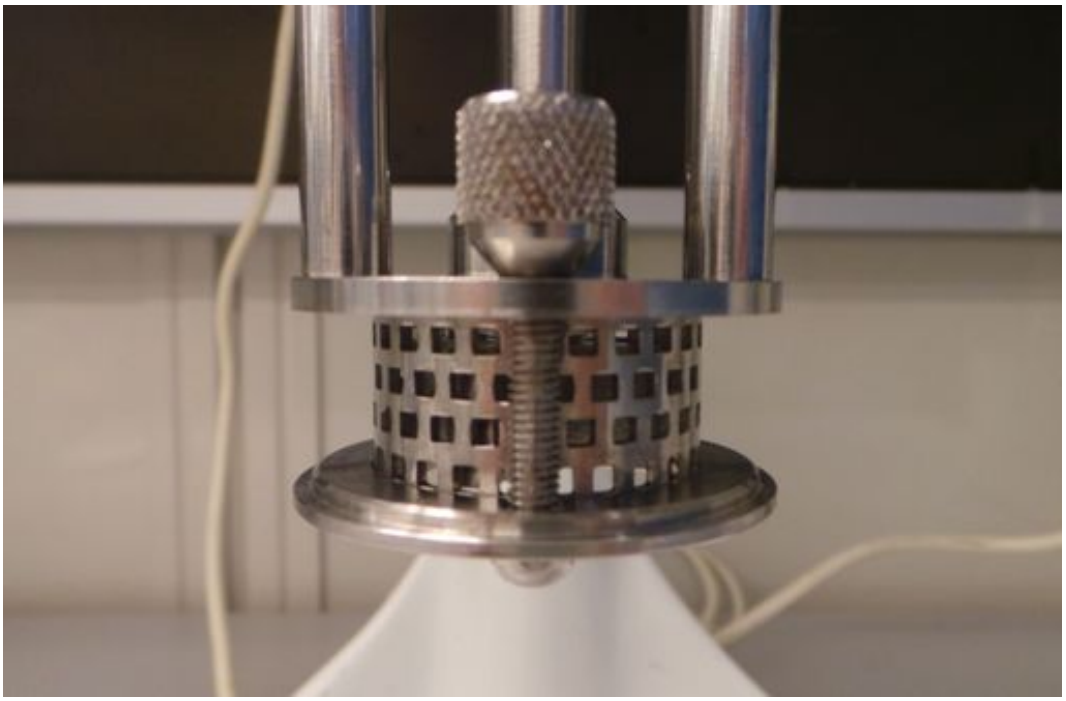

Figure C.7: Square Hole High Shear Screen workhead